Spectral distortions and anisotropies of the Cosmic Microwave Background

Gianfranco De Zotti[1,2] and Mattia Negrello[1]

1. INAF-Osservatorio Astronomico di Padova,
   Vicolo dell'Osservatorio 5, I-35122 Padova, Italy
2. SISSA, Via Bonomea 265, 34136, Trieste, Italy

This contribution presents a synthetic review of the theory and the observations on spectral distortions and on anisotropies of the Cosmic Microwave Background (CMB). For a better understanding of the content of these lectures, it is useful to refer also to the figures contained in the slides available on the School's website.

1 Introduction

Fifty years after the report of the discovery of the Cosmic Microwave Background (CMB; Penzias & Wilson, 1965; Dicke et al., 1965) and 25 years after the first report of CMB spectral measurements by the Far Infrared Absolute Spectrophotometer (FIRAS) on the Cosmic Background Explorer (COBE) satellite (Mather et al., 1990), deviations from a perfect black-body have still to be detected. Yet, since the Universe is obviously not in thermal equilibrium, the CMB spectrum cannot be exactly Planckian.

No substantial progress was made on CMB spectral measurements after COBE/FIRAS, while theoretical investigations on physical mechanisms that can produce spectral distortions have been actively continuing. Unavoidable CMB spectral distortions have been discussed by Sunyaev & Khatri (2013) who pointed out that some of them, which carry information on the cosmic history inaccessible by any other means, must be present at a level accessible to modern technology. And indeed there are projects, such as the proposed Primordial Inflation Explorer (PIXIE; Kogut et al., 2014) that promise improvements in measurement accuracy by 2–3 orders of magnitude compared to COBE/FIRAS. The theory of spectral distortions and the current observational constraints are summarized in Sect. 2.

On the contrary, the last several years have seen a spectacular progress in the mapping of CMB anisotropies, thanks to ground based, balloon borne and satellite experiments. This has allowed us to determine the parameters of the cosmological model with unprecedented precision and to put on a solid basis models for the evolution of the large-scale structure. In Sect. 3 we review some of the basics of CMB anisotropies and summarize the main recent results.

2 Spectral distortions

The CMB spectral distortions that may be expected as the result of processes occurring in the early universe have been characterized primarily by Zeldovich and Sunyaev

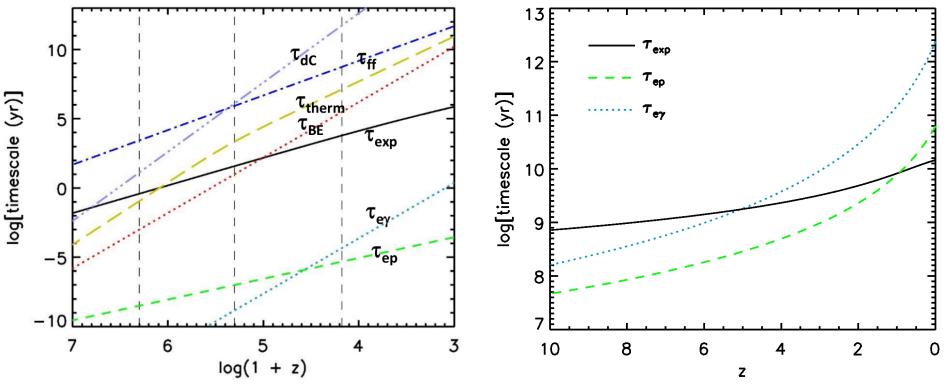

Fig. 1: **Left-hand panel:** timescales of processes governing the evolution of CMB distortions compared with the expansion timescale (thick black solid line) before recombination. **Right-hand panel:** timescales for thermal equilibrium between electrons and the radiation field and between electrons and protons in the post-reionization era; $\tau_{\rm ep}$ was computed adopting the cosmic number density of baryons and an electron temperature $T_e = 10^7$ K.

(Zeldovich & Sunyaev, 1969; Sunyaev & Zeldovich, 1970; Zel'dovich et al., 1972; Sunyaev, 1974; Illarionov & Sunyaev, 1975a,b). The evolution of distorted spectra and constraints on processes that can produce them have been investigated, both analytically and numerically, by numerous subsequent studies (see reviews by Danese & de Zotti, 1977; Sunyaev & Zeldovich, 1980; Burigana, 1993; Sunyaev & Khatri, 2013; Chluba, 2014).

2.1 Time scales

Useful insights into the processes governing the evolution of the CMB spectrum come from consideration of interaction timescales, compared with the cosmic expansion timescale, $\tau_{\rm exp}$ (see the left-hand panel of Fig. 1). For a flat ΛCDM universe we have:

$$\tau_{\rm exp} = \frac{a(t)}{\dot{a}(t)} \simeq \frac{4.56\times10^{17}}{\left[\Omega_m(1+z)^3+\Omega_r(1+z)^4+\Omega_\Lambda\right]^{1/2}}\ {\rm s}, \tag{1}$$

where $\Omega_r = 1.68\, a_{\rm BB}\, T_{\rm CMB}^4/\rho_{\rm cr} \simeq 9.05\times10^{-5}$, $a_{\rm BB} = 7.56\times10^{-15}\,{\rm erg\,cm^{-3}\,K^{-4}}$ being the black-body constant and $\rho_{\rm cr} = 8.61\times10^{-30}\,{\rm g\,cm^{-3}}$. The factor 1.68 takes into account relativistic neutrinos. Here and in the following we adopt $H_0 = 67.7\,{\rm km\,s^{-1}\,Mpc^{-1}}$ (Planck Collaboration, 2015d); obviously, $\tau_{\rm exp} \propto 1/H_0$.

In the pre-recombination plasma, the relaxation time for thermal equilibrium between electrons and protons, ($\tau_{\rm ep}$, Spitzer, 1962),

$$\tau_{\rm ep} \simeq 2.8\times10^8 \left(\frac{T_e}{T_r}\right)^{3/2} (1+z)^{-3/2}\ {\rm s}, \tag{2}$$

is much shorter than $\tau_{\rm exp}$ so that the two constituents of the plasma are kept at the same temperature.

The coupling of the plasma with the radiation field is governed by Compton (Thomson) scattering. The Compton cooling time of hot electrons, $\tau_{e\gamma}$, is

$$\tau_{e\gamma} = \frac{3m_e c}{4\sigma_T \epsilon_r} \simeq 7.4 \times 10^{19}(1+z)^{-4} \text{ s}, \tag{3}$$

where σ_T is the Thomson cross section and $\epsilon_r = aT_r^4$. Before recombination $\tau_{e\gamma}$ is much shorter than the free-free cooling time

$$t_{\rm ff} = \frac{3n_e kT_e}{w_{\rm ff}} \simeq 9.6 \times 10^{17} C^{-1} \left(\frac{\bar{g}(T_e)}{1.2}\right)^{-1} T_e^{1/2}(z)(1+z)^{-3} \text{ s}, \tag{4}$$

where

$$w_{\rm ff} = 9.5 \times 10^{-41} C \left(\frac{\bar{g}(T_e)}{1.2}\right) T_e^{1/2}(z)(1+z)^6 \text{ erg s}^{-1}\text{ cm}^{-3}, \tag{5}$$

is the free-free energy loss rate by a fully ionized plasma with cosmological composition, $C = \langle n_e^2\rangle/\langle n_e\rangle^2$ is the clumping factor ($\langle ...\rangle$ denotes average values) and $\bar{g}(T_e)$ is the frequency average of the velocity averaged Gaunt factor, whose values are in the range 1.1 to 1.5 (Rybicki & Lightman, 1979).

Before recombination $\tau_{e\gamma}$ is also much shorter than $\tau_{\rm exp}$. The very large dimensionless specific photon entropy (photon entropy per electron divided by the Boltzmann constant k)

$$s = \frac{4a_{\rm bb}T_{\rm CMB}^3}{3n_e K} \simeq 6.72 \times 10^9, \tag{6}$$

ensures that the radiation acts as a powerful thermostat, keeping electrons and protons at the equilibrium temperature with the radiation field (Peyraud, 1968; Zel'dovich & Levich, 1970).

The situation is different in the reionization era ($z < z_{\rm reion}$). As illustrated by the right-hand panel of Fig. 1, $\tau_{e\gamma}$ exceeds $\tau_{\rm exp}$ for $z \leq 5$. Thus keeping the universe fully ionized at $z \gg 5$ becomes increasingly demanding in terms of energetics. For realistic values of the clumping factor ($C \sim 3$, Kuhlen & Faucher-Giguère, 2012), the cooling by free-free is always sub-dominant.

After reionization the plasma can be heated to very hight temperatures (see sub-Sect. 2.9) and

$$\tau_{\rm ep} \simeq 1.95 \times 10^{18} \left(\frac{T_e}{10^7\,\text{K}}\right)^{3/2} (1+z)^{-3} \text{ s}, \tag{7}$$

can become comparable to, or even larger than $\tau_{\rm exp}$ for z of a few units (right-hand panel of Fig. 1). Thus electron and protons could have different temperatures.

2.2 Bose-Einstein (μ-type) distortions

The photon-electron collision time is

$$\tau_{\gamma e} = (n_e \sigma_T c)^{-1} \simeq 2.3 \times 10^{20}(1+z)^{-3} \text{ s}. \tag{8}$$

The mean energy gain of a photon by inverse Compton scattering is $kT_e/m_e c^2$ and the characteristic time for the establishment of a quasi-equilibrium spectrum by effect

of the inverse Compton scattering is:

$$\tau_{\rm BE} = \tau_{\gamma e} \left(\frac{kT_e}{m_e c^2} \right)^{-1} \simeq 5 \times 10^{29} \frac{T_r}{T_e} (1+z)^{-4} \ {\rm s}. \tag{9}$$

The quasi-equilibrium solution is a Bose-Einstein spectrum with photon occupation number

$$\eta_{\rm BE} = \frac{1}{e^{x_e+\mu} - 1}, \tag{10}$$

with

$$x_e = \frac{h\nu}{kT_e} \simeq 1.761 \frac{\nu}{100{\rm GHz}} \frac{T_r}{T_e} \tag{11}$$

so that $x_e = 1$ corresponds to $\nu_e \simeq 56.786 (T_e/T_r)$ GHz. The equilibrium electron temperature in such radiation field is slightly higher than the radiation temperature: $T_e \simeq T_r(1 + 0.456\mu)$, for $\mu \ll 1$.

2.3 Thermalization of the CMB spectrum

So far photon-producing processes have been neglected. However, although their electron cooling rate is small compared to inverse Compton, they do have an important role. The main photon-producing processes are the free-free and double Compton scattering, whose characteristic timescales for the evolution of the photon occupation number are

$$\tau_{\rm ff} = 4.8 \times 10^{26} (1+z)^{-5/2} \ {\rm s} \tag{12}$$

and

$$\tau_{\rm dC} = 1.3 \times 10^{40} (1+z)^{-5} \ {\rm s}. \tag{13}$$

The latter is therefore dominant at very high redshifts.

While the characteristic time for Compton diffusion is frequency-independent, the timescales for free-free or double Compton absorption are

$$\tau_{\rm abs\,ff,dC} = \tau_{\rm ff,dC} \frac{x_e^3 \exp(x_e)}{g_{\rm ff,dC}[\exp(x_e) - 1]}, \tag{14}$$

where $g_{\rm ff}$ and $g_{\rm dC}$ are the free-free and double Compton Gaunt factors that, assuming a pure hydrogen plasma, can be approximated by (Draine, 2011)

$$g_{\rm ff}(\nu, T_e) = \ln \left\{ \exp \left[5.960 - \frac{\sqrt{3}}{\pi} \ln \left(\frac{\nu}{\rm GHz} \left(\frac{T_e}{10^4 {\rm K}} \right)^{-1.5} \right) \right] + \exp(1) \right\}, \tag{15}$$

and (Chluba & Sunyaev, 2012)

$$g_{\rm dC}(\nu, T_e) = \left(1 + \frac{3}{2}x + \frac{29}{24}x^2 + \frac{11}{16}x^3 + \frac{5}{12}x^4 \right) e^{-2x}. \tag{16}$$

The photon absorption timescale decreases as x_e^2 for $x_e \ll 1$ and becomes shorter than $\tau_{\rm BE}$ for $x_e < x_c$ with

$$x_c = \tau_{\rm BE}^{1/2} \left(\frac{g_{\rm ff}}{\tau_{\rm ff}} + \frac{g_{\rm dC}}{\tau_{\rm dC}} \right)^{1/2}. \tag{17}$$

For $x_e > x_c$ photons are scattered to higher frequencies before they can be absorbed while for $x_e < x_c$ photon absorption is faster and an equilibrium spectrum is established. The solution of the kinetic equation including both Compton scattering and photon emitting processes has a frequency dependent chemical potential

$$\mu(x_e) = \mu_0 e^{-x_c/x_e}. \tag{18}$$

At early enough times the cooperation of photon-emitting processes, that mostly produce low-frequency photons, and of Compton scattering that moves them up in frequency, leads to complete thermalization of the distortions. The thermalization timescale is

$$\tau_{\rm th} = \left(\frac{\tau_{\rm BE}}{1/\tau_{\rm ff} + 1/\tau_{\rm dC}} \right)^{1/2}. \tag{19}$$

A rough approximation of the thermalization redshift is obtained setting $\tau_{\rm th} \simeq \tau_{\rm exp}$. The detailed study by Khatri & Sunyaev (2012) yielded $z_{\rm th} \simeq 2 \times 10^6$.

What about cyclotron emission? Possible imprints of a stochastic background of primordial magnetic fields (PMFs) on CMB anisotropies, on CMB polarization and on non-Gaussianities were investigated by Planck Collaboration (2015e) using *Planck* data. The derived 95% confidence upper limits on the present day comoving magnetic field value, B_0, at a scale of 1 Mpc assuming magnetic flux freezing [$B = B_0(1+z)^2$] were found to be $B_{1\,\rm Mpc} < 5.6\,{\rm nG}$ (see also Chluba et al., 2015a).

In the case of thermal electrons, the cyclotron energy loss rate is (Tortia, 1961):

$$w_{\rm cycl} = \frac{4}{3} \frac{e^4 B^2 n_e}{m_e^3 c^5} k T_e \sim 10^{-48} \left(\frac{B_0}{5\,{\rm nG}} \right)^2 \frac{T_e}{T_r} (1+z)^8 \,{\rm erg\,cm^{-3}\,s^{-1}}. \tag{20}$$

Its ratio with the free-free energy loss rate [eq. (5)] is, taking into account that at high redshifts $C \simeq 1$

$$\frac{w_{\rm ff}}{w_{\rm cycl}} \simeq 1.95 \times 10^7 \left(\frac{\bar{g}(T_e)}{1.2} \right) \left(\frac{T_e}{T_r} \right)^{-1/2} \left(\frac{B_0}{5\,{\rm nG}} \right)^{-2} (1+z)^{-1.5}, \tag{21}$$

suggesting that, if B is not too far from its upper limit, the cyclotron emission may be the dominant photon producing process at high z (Afshordi, 2002). However Zizzo & Burigana (2005) showed that in fact cyclotron has a negligible impact on the evolution of spectral distortions. This is because photons are emitted at very low frequencies. The characteristic dimensionless frequency is

$$x_{\rm e,cycl} \simeq 2.5 \times 10^{-13} \left(\frac{T_e}{T_r} \right)^{-1} \left(\frac{B_0}{5\,{\rm nG}} \right) (1+z), \tag{22}$$

much lower, for values of B_0 consistent with observational constraints, than the frequency x_c at which an equilibrium spectrum is established by the free-free and double Compton ($x_c > 5 \times 10^{-3}$).

A rough estimate of the minimum redshift at which μ-type distortions can be produced is obtained from $\tau_{\rm BE} \simeq \tau_{\rm exp}$, giving $z_{\rm BE,min} \simeq 10^5$. The precise calculations by Khatri et al. (2012a,b) gave $z_{\rm BE,min} = 2 \times 10^5$.

2.4 Weak Comptonization (y-type) distortions

When $\tau_{\rm exp}/\tau_{\rm BE} \lesssim 0.01$ ($z \lesssim 1.5 \times 10^4$; Khatri et al., 2012a,b), i.e. in the weak Comptonization limit, the distortions convey some information on the mechanism of energy release: the shape of the distorted spectrum is slightly different depending on whether there is direct electron heating or the energy is released to the radiation field. Setting:

$$y(t) = \int_{t_0}^{t} \frac{{\rm d}t'}{t_{\rm BE}}, \tag{23}$$

and $x = h\nu/kT$, T being the temperature of a black-body with the same photon number density as the actual radiation field, the Compton term of the Kompaneets (1957) equation writes:

$$\frac{\partial \eta}{\partial y} = \frac{1}{x^2}\frac{\partial}{\partial x}\left\{x^4\left[\frac{\partial \eta}{\partial x}\right]\frac{T_e}{T} + \eta(x) + \eta^2(x)\right\}. \tag{24}$$

In the case of small distortions

$$\eta(x) \simeq \eta_{\rm Planck}(x) = \frac{1}{e^x - 1}, \tag{25}$$

so that

$$\frac{\partial \eta}{\partial x} \simeq -[\eta(x) + \eta^2(x)], \tag{26}$$

and the Compton term can be approximated by the "diffusion" equation

$$\left(\frac{\partial \eta}{\partial u}\right)_C \simeq \frac{1}{x^2}\frac{\partial}{\partial x}\left[x^4\frac{\partial \eta}{\partial x}\right]. \tag{27}$$

with

$$u(t) = \int_{t_0}^{t}\left(\frac{T_e}{T_r} - 1\right)\frac{{\rm d}t'}{t_{\rm EB}}. \tag{28}$$

With a suitable change of variable (Danese & de Zotti, 1977) this equation takes the form of the one-dimensional heat conduction whose solution is (Zeldovich & Sunyaev, 1969)

$$\eta(x,y) = \frac{1}{(4\pi y)^{1/2}}\int_0^\infty \eta_i(x',0)\exp\{-\frac{1}{4y}\ln^2[\frac{x}{x'}\exp(3y)]\}\frac{dx'}{x'}, \tag{29}$$

which holds for any initial radiation spectrum $\eta_i(x,0)$. If $yx^2 \ll 1$ and the initial spectrum is black-body eq. (29) simplifies to (Zeldovich & Sunyaev, 1969)

$$\eta_C(x,y) = \eta_{\rm P}(\tilde{x})\big[1 + y\frac{\tilde{x}\exp(\tilde{x})}{\exp(\tilde{x}) - 1}\big(\frac{\tilde{x}}{\tanh(\tilde{x}/2)} - 2\big)\big], \tag{30}$$

where $\tilde{x} = x(T_{\rm CMB}/T_{\rm RJ})$ with $T_{\rm RJ} = T_{\rm CMB}\exp(-2y)$ and $\tanh(x) = [\exp(2x) - 1]/[\exp(2x) + 1]$. Equation (30) shows that the weak Comptonization decreases the CMB temperature at low frequencies (in the Rayleigh-Jeans region we have $(T_{\rm RJ} - T_{\rm CMB})/T_{\rm CMB} \simeq -2y$). The signal $\Delta T/T$ vanishes at 217 GHz and at higher frequencies we have an excess over the black-body spectrum.

More generally, the distorted spectrum in the weak Comptonization case can be described by a superposition of black-body spectra

$$\eta(x,y) = \int_0^\infty R(T,y)\eta_{\rm Planck}(\nu,T)\,{\rm d}T\,. \tag{31}$$

The temperature distribution function depends on the specific heating process. One example, referring to electron heating, was shown above. But important processes that occur in the early universe, such as dissipation of adiabatic density perturbations, may result in distortions generated by intermixing of photons coming from plasma clouds having macroscopic relative velocities without direct electron heating. The temperature distribution seen by an external observer in the case of clouds with a Maxwellian velocity distribution, each containing radiation at the same temperature T_r, is (Zel'dovich et al., 1972):

$$R(T,w) = \frac{1}{T_r\sqrt{4\pi w}}\exp\left[-\frac{1}{4w}\left(\frac{T}{T_r}-1\right)^2\right], \tag{32}$$

where $w = \langle\beta^2\rangle/6$, $\langle\beta^2\rangle$ is the velocity dispersion of the clouds in units of c.

Even for very low values of the parameters y and w ($y, w \sim 1\times10^{-8}$) the spectra given by eq. (29) and by eq. (31) plus eq. (32) should be distinguishable by the PIXIE experiment (Kogut et al., 2014). The spectrum given by the approximate solution of eq. (30) is indistinguishable, for the considered value of y, from that given by eq. (29).

2.5 Intermediate epoch distortions

CMB spectral distortions generated after the epoch of BE distortions and before that of weak Comptonization, i.e. in the redshift range $1.5\times10^4 \lesssim z \lesssim 2\times10^5$, have been investigated in detail by Khatri et al. (2012b). These authors have shown that these intermediate epoch distortions provide much more information than μ– and y–type distortions.

While the latter are informative mainly on the amount of energy injected into the CMB, the shape of the former depends sensitively on the redshift of energy injection and allows us to distinguish among the mechanisms that have been operating, for example between particle annihilation and Silk damping.

2.6 Sources of spectral distortions

Spectral distortions produced by physical processes that must have occurred during the history of the Unverse have been thoroughly reviewed by Sunyaev & Khatri (2013) and Chluba (2014); for more recent work see Chluba et al. (2015b) and references therein.

Here we only remind a point that, although not new, is less well known. Even in the absence of energy injections, small spectral distortions occur. When baryons are non-relativistic, their adiabatic index is 5/3. This causes the baryon temperature to be proportional to $(1+z)^2$ so that they cool faster than CMB photons. But, as long as electrons are tightly coupled with the radiation field, photons keep heating up the baryons. Thus the radiation temperature evolves not as $T_{\rm CMB} \propto (1+z)$ but

approximately as $T_R \propto (1+z)^{1+\epsilon}$ (Danese & de Zotti, 1977) with

$$\epsilon = \frac{3 n_e K}{4 a_{\rm bb} T_{\rm CMB}^3} = s^{-1} \simeq 1.49 \times 10^{-10}, \tag{33}$$

s being the dimensionless specific photon entropy [eq. (33)]. If T_i is the CMB temperature at the minimum redshift, z_i, at which thermalization of spectral distortions is ensured and $T_{\rm bb} = T_i(1+z)/(1+z_i)$ is the blackbody temperature corresponding to the photon number density we have

$$\begin{aligned} \Delta T \equiv T_{\rm bb} - T_R &= T_i \left[\frac{1+z}{1+z_i} - \left(\frac{1+z}{1+z_i} \right)^{1+\epsilon} \right] \\ &\simeq T_i \left[\frac{1+z}{1+z_i} - \frac{1+z}{1+z_i} - \frac{1+z}{1+z_i} \ln \left(\frac{1+z}{1+z_i} \right) \epsilon \right], \end{aligned} \tag{34}$$

i.e. (Khatri et al., 2012a)

$$\frac{\Delta T}{T_{\rm CMB}} = \ln \left(\frac{1+z}{1+z_i} \right) \epsilon \tag{35}$$

and $\Delta E/E_{\rm bb} \simeq 4(\Delta T/T_{\rm bb})$. The photon cooling results in an *excess* of photons compared to a perfectly black-body spectrum. Detailed calculations (Chluba & Sunyaev, 2012; Khatri et al., 2012a) have shown that the resulting spectrum has a μ-type distortions at GHz frequencies and a y-type distortion at high frequencies but with *negative* values of the parameters. The distortions are tiny ($\mu_0 \sim -2\times10^{-9}$, $y \sim -4.3\times10^{-10}$). Those of y-type are easily swamped by the much larger *positive* distortions expected at low z. Those of μ-type may partially or even entirely cancel the positive μ distortions created by dissipation of acoustic waves on small scales due to photon diffusion (Khatri et al., 2012a).

The photon cooling via Compton scattering moves the excess photons to lower and lower frequencies. However, as shown by Khatri et al. (2012a), this does not lead to a Bose–Einstein condensation because the process is slow enough that the condensed photons are efficiently absorbed by double Compton scattering and free-free.

2.7 Foregrounds

Figure 2 shows up-to-date estimates of Galactic and extragalactic foreground spectra. The average Galactic emissions at latitudes $|b| > 30^\circ$ and $|b| > 50^\circ$ have been obtained using an updated version of the Planck Sky Model (PSM; Delabrouille et al., 2013) that incorporates the recently published measurements by the *Planck* satellite (Planck Collaboration, 2014a,b, 2015h,g).

The PSM aims at providing a simulation of the sky as realistic as possible over a broad frequency range. It includes, in addition to a model of the CMB, Galactic diffuse emissions (synchrotron, free-free, thermal and spinning dust, CO lines), Galactic HII regions, extragalactic radio sources, dusty galaxies, the Cosmic Infrared Background (CIB), thermal and kinetic Sunyaev-Zeldovich signals from clusters of galaxies. Each component is simulated by means of educated interpolations/extrapolations of the available data, complemented by state-of-the-art models.

Distinctive features of the simulations are spatially varying spectral properties of synchrotron and dust; different spectral parameters for each point source; modelling

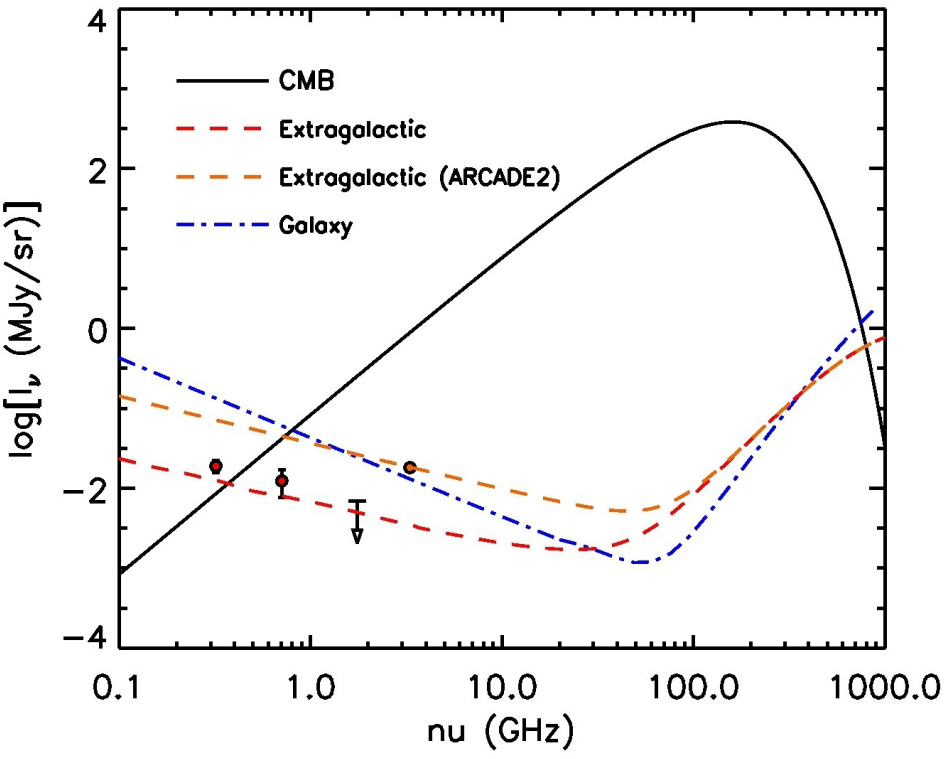

Fig. 2: Galactic and extragalactic foreground intensity compared with the CMB spectrum, assumed to be a perfect blackbody at $T = 2.725\,\mathrm{K}$. The dot-dashed blue line shows the intensity of Galactic emissions (including synchrotron, free-free, spinning dust and thermal dust) averaged over latitudes $|b| > 50^\circ$, based on an updated version of the Planck Sky Model (Delabrouille et al., 2013). The two dashed (red and orange) lines shows two estimates of the spectrum of extragalactic foregrounds. The two estimates differ at low frequencies (left-hand part of the figure). The lower dashed (red) curve, obtained from the observed source counts, is consistent with observational estimates by Wall et al. (1970) at 0.32 GHz and 0.707 GHz, and by Vernstrom et al. (2015) at 1.75 GHz, claimed to be an upper limit (see de Zotti et al., 2010, for a review). The upper dashed orange curve shows the the ARCADE 2 estimates (Fixsen et al., 2011) based on their new measurement at 3.3 GHz (black circle) and on a re-analysis of earlier data. At high frequencies both lines show the spectrum of the Cosmic Infrared Background (CIB) determined by (Fixsen et al., 1998).

of the clustering properties of extragalactic sources and of the power spectrum of CIB fluctuations, in close agreement with the latest observational determinations.

As illustrated by Fig. 2, foreground emissions dominate below $\sim 0.8\,\mathrm{GHz}$ and above $\sim 800\,\mathrm{GHz}$. Their intensity is always orders of magnitude above the PIXIE sensitivity, implying that a full exploitation of the potential of this experiment to pin down spectral distortions several orders of magnitude weaker than the current COBE/FIRAS upper limits will require an extremely refined foreground subtraction.

In the PIXIE frequency range, the dominant extragalactic foreground is the CIB. Its subtraction will be complicated by spectral bumps due to the integrated emission of strong far/IR–mm wave lines such as the CO and the CII $157.7\,\mu$m lines produced by star-forming galaxies. Contributions from these lines can be of a few percent of the CIB. On the other hand, the PIXIE spectral coverage with many frequency channels is optimally suited for the foreground subtraction purpose. And the accurate measurements of the CIB spectrum that PIXIE can provide are important *per se*. In fact, the current uncertainty on the CIB spectrum is one of the main limitations to a full understanding of the energetics of dust-obscured star formation and AGN accretion.

2.8 Comptonization distortions from re-ionization

2.8.1 Short historical notes

Already very weak constraints on distortion parameters ($y \leq 0.15$), combined with an upper limit of 1 K to the brightness temperature of the free-free emission from the inter-galactic plasma at 600 MHz, allowed Sunyaev (1968) and Zeldovich & Sunyaev (1969) to infer "The necessity of a neutral hydrogen period in the evolution of the universe", provided that the density parameter is not too low. An absolute upper limit to the re-ionization redshifts was $z_{\rm max} \simeq 300\Omega^{-7/9}$ or, distinguishing between Ω and Ω_b (at the time the dark matter, and even less the dark energy, were not yet within the astrophysicists' horizon),

$$z_{\rm max} < 300 \left(\frac{\delta I_{\rm ff}(600\,\mathrm{MHz})}{10^{-2}\mathrm{MJy\,sr^{-1}}}\right)^{4/9} \left(\frac{y}{0.15}\right)^{2/9} \Omega_b^{-10/9}\Omega^{1/3}. \quad (36)$$

The constraints on CMB distortions improved slowly. Illarionov & Sunyaev (1975b) estimated an observational upper limit in the range $y < 0.04$–0.1. Field & Perrenod (1977) estimated a 90% confidence interval $0.013 < y < 0.05$ primarily based on the balloon measurements by Woody et al. (1975). This value of y was shown to be consistent with the X-ray background being bremsstrahlung emission from a hot ($T \simeq 4.4 \times 10^8\,\mathrm{K}$), dense ($\Omega_b \simeq 0.46$) IGM. The statistical analysis by Danese & de Zotti (1978) yielded $y < 0.05$ (excluding the data by Woody et al. (1975)) and $\mu < 0.01$.

New support to the case for a relatively large Comptonization distortion ($y = 0.02 \pm 0.002$; Smoot et al., 1988) was provided by the sounding rocket measurements by Matsumoto et al. (1988), although the measurements of the balloon-borne experiment by Peterson et al. (1985) did not detect significant deviations from a black-body spectrum at wavelengths down to 0.9 mm.

This was the situation close to the COBE launch date (November 18th, 1989) and the appearance of the first FIRAS results (Mather et al., 1990) that have revolution-

ized the field. Indications of comptonization distortions were rejected and constraints on distortion parameters were improved by three orders of magnitude ($|y| < 1.5 \cdot 10^{-5}$ and $|\mu_0| < 9 \cdot 10^{-5}$; Fixsen et al., 1996).

Subsequent work concerned long wavelengths, outside the FIRAS range. The main improvements were on free-free distortions, while those on μ were only marginal. The latest constraints at 95% C.L. are (Gervasi et al., 2008) $|\mu| < 6 \times 10^{-5}$ and $-6.3 \times 10^{-6} < Y_{ff} < 12.6 \times 10^{-6}$ where Y_{ff} is the optical depth to free-free emission, yielding an excess antenna temperature given by:

$$\Delta T_{\rm ff} = T_{\rm CMB}\ \frac{Y_{ff}}{x^2}, \tag{37}$$

i.e. $-0.15 < \Delta T_{\rm ff}/{\rm K} < 0.31$ or $\delta I_{\rm ff}(600\,{\rm MHz}) < 3.4 \times 10^{-3}\,{\rm MJy\,sr^{-1}}$.

Weaker constraints were set by the ARCADE 2 measurements; Seiffert et al. (2011) argue that the constraints by Gervasi et al. (2008) are likely too optimistic because the fit to the data was too constrained. With the tightest present contraints [$|y| < 1.5 \cdot 10^{-5}$ and $\Delta T_{\rm ff}(600{\rm MHz}) < 0.31\,{\rm K}$] the argument by Zeldovich & Sunyaev (1969) gives $z_{\rm max} < 37\Omega_b^{-2/3}\Omega^{1/3}(10^4\,{\rm K}/T_e)^{2/3}$, showing that current sensitivities to both the y parameter and to the free-free emission of the re-ionized IGM do not reach the levels expected from our current understanding of the re-ionization history.

2.9 Re-ionization distortions

The most recent determination of the electron scattering optical depth due to re-ionization is $\tau_{\rm es} = 0.066 \pm 0.016$ (Planck Collaboration, 2015d). Then if, to get the order of magnitude of the y parameter due to re-ionization, we take an approximately constant electron temperature we have:

$$\begin{aligned} y_{\rm reion} &= \int n_e \sigma_T c \frac{k\,T_e}{m_e\,c^2} dt \simeq \frac{k\,T_e}{m_e\,c^2}\tau_{\rm es} \simeq \frac{T_e}{5.93 \times 10^9\,{\rm K}}\tau_{\rm es} \\ &\simeq 2.2 \times 10^{-7} \left(\frac{\tau_{\rm es}}{0.066}\right)\left(\frac{T_e}{2 \times 10^4{\rm K}}\right), \end{aligned} \tag{38}$$

where $2 \times 10^4\,{\rm K}$ corresponds to the peak of the hydrogen cooling curve (Sutherland & Dopita, 1993).

The corresponding energy transfer to the CMB is

$$\begin{aligned} \Delta\epsilon &\simeq 4y\epsilon_r \simeq 3.7 \times 10^{-19} \left(\frac{\tau_{\rm es}}{0.066}\right)\left(\frac{T_e}{2 \times 10^4{\rm K}}\right)\,{\rm erg\,cm^{-3}} \\ &\simeq 1.9 \times 10^{-5}\epsilon_{\rm EBL} \simeq 1.2 \times 10^{-4}\epsilon_{\rm AGN}, \end{aligned} \tag{39}$$

$\epsilon_{\rm EBL} \simeq 2 \times 10^{-14}\,{\rm erg\,cm^{-3}}$ (Dole et al., 2006) being the radiation energy density produced by thermonuclear reactions in stars and $\epsilon_{\rm EBL} \simeq 3 \times 10^{-15}\,{\rm erg\,cm^{-3}}$ that produced by nuclear activity. The latter quantity has been estimated in two ways: from the energy density of the X-ray background adopting a bolometric correction of a factor of 20 and from the present day black hole mass density $\rho_{\rm BH} \simeq 4.5 \times 10^5\,{\rm M_\odot\,Mpc^{-3}}$ (Shankar et al., 2009) via the equation

$$\epsilon_{\rm AGN} = \frac{\eta_{\rm AGN}}{1 - \eta_{\rm AGN}}\rho_{\rm BH}c^2, \tag{40}$$

adopting the standard matter to radiation conversion efficiency $\eta_{\rm AGN} = 0.1$. Both methods give a similar result.

Thus a small fraction of the energy produced by nuclear reactions in stars and/or by nuclear activity coming out in mechanical form and going into heating of the IGM is enough to raise the electron temperature to values much higher than $T_e \simeq 1$–2×10^4 K, the value expected by effect of the ionizing radiation.

Current galaxy evolution models advocate strong feedback effects from supernova explosions and from Active Galactic Nuclei (AGNs), generating superwinds. Such feedback effects are felt responsible for the differences in shape between the halo mass function and the galaxy luminosity or stellar mass functions (e.g. Silk & Mamon, 2012). They may heat a substantial fraction ($\sim$ 40–50% according to Cen & Ostriker, 2006) of the IGM to 10^5–10^7 K. Note however that the simulations by Tornatore et al. (2010), including different feedback recipes, indicate that 90% of the baryonic mass at $z > 3.5$ has T in the range 10^4–10^5 K; the fraction decreases to $\simeq 75\%$ at $z = 2$ and to $\simeq 50\%$ at $z = 1$.

Most AGN feedback models imply that $\simeq 5\%$ of the AGN bolometric emission is a mechanical form (Lapi et al., 2005, 2006; Zubovas & King, 2012). There is ample and mounting observational evidence of AGN-driven galaxy superwinds (Fabian, 2012). Harrison et al. (2012) find outflow powers $\sim$ 0.2–5% of the AGN luminosities, but with large uncertainties; Genzel et al. (2014) report evidence of widespread AGN-driven ionized outflows in the most massive star-forming galaxies at $z = 1$–3; Brusa et al. (2015) find lower limits to the ratio of the kinetic to bolometric luminosity of the AGN nucleus in the range 0.1–5% for a sample of $z \sim 1.5$ X-ray selected, obscured QSOs.

According to Zubovas & King (2012) the energy-driven superwinds originated in the immediate vicinity of the active nucleus shock-heat the ISM creating a two-phase medium in which molecular species (cold phase, comprising only $\sim$ 10% of the gas) co-exist with hot gas. The large-scale outflows generated by super-winds are capable of driving the ISM out of the galaxy potential well. Their energy is then dissipated in the IGM.

Using the redshift-dependent mean luminosity density $\rho_L(z)$ (inset in Fig. 1 of Aversa et al., 2015) we estimated the mean electron temperature, T_e, given the fraction of ρ_L, ϵ_h, that goes into heating of the IGM, by solving the equation:

$$\frac{{\rm d}T_e(z)}{{\rm d}t} = \frac{\epsilon_h \rho_L(z)}{3 n_e k} - \frac{T_e}{\tau_{\rm e\gamma}} - \frac{2T_e}{\tau_{\rm exp}}, \tag{41}$$

where $\tau_{\rm e\gamma}$ is the cooling time of electrons by inverse Compton scattering, given by eq. (3). The last term in the right-hand side accounts for the cooling by adiabatic expansion, with timescale $\tau_{\rm exp}$ given by eq. (1). We have neglected the cooling by free-free emission whose rate is about two orders of magnitude lower than that of Compton cooling (see sub-Sect. 2.1).

For the standard $\epsilon_h = 0.05$ we find mean electron temperatures, T_e, in the range 10^5–10^6 at $z = 1$–3, when the AGN activity peaks. Once we have $T_e(z)$ we can compute

$$y_{\rm reion} \;=\; \int n_e \sigma_T c \frac{k\, T_e(z)}{m_e\, c^2} dt$$

$$\simeq \quad 3.36\times10^{-6}\int_0^{z_{\rm reion}}{\rm d}z\left(\frac{T_e(z)}{10^7\,{\rm K}}\right)\frac{(1+z)^2}{\sqrt{\Omega_m(1+z)^3+\Omega_{\rm rad}(1+z)^4+\Omega_\Lambda}}. \quad (42)$$

We get $y_{\rm reion}\simeq 2\times10^{-6}$, the main contribution coming from $z\lesssim 3$.

Some data indicate substantially higher values of $y_{\rm reion}$. Van Waerbeke et al. (2014) report a correlation between gravitational lensing by large scale structure and the thermal Sunyaev-Zeldovich (SZ) effect consistent with a warm plasma of temperature $\simeq 10^6\,{\rm K}$ and a comoving electron number density $n_e\simeq 0.25\,{\rm m}^{-3}$ at $z\simeq 4$. If this temperature remains constant down to $z=0$ this implies $y\geq 4\times10^{-6}$.

Ruan et al. (2015) report the detection of a strong signal at $>5\,\sigma$ significance by stacking thermal SZ Compton-y maps centered on the locations of 26,686 spectroscopic quasars. They interpret the signal as due to thermal feedback energetics amounting to 5% of the black hole mass, i.e. to $\simeq 50\%$ of the AGN bolometric luminosity if $\eta_{\rm AGN}=0.1$. In this case we obtain mean electron temperatures, T_e, in the range 10^6–10^7 at $z=1$–3 and $y\simeq 10^{-5}$, only marginally below the COBE/FIRAS upper limit.

An additional contribution to y comes from shocks associated to structure formation. Assuming that the shocks generated by the collapse and virialization process efficiently heats up the baryons (e.g. Moss & Scott, 2009) we get $y\simeq 10^{-6}$, in agreement with the earlier estimate by Nath & Silk (2001).

We conclude that $y_{\rm reion}\simeq$ several $\times\,10^{-6}$, i.e. is not much below the current upper limit, may be expected.

The free-free emission associated to the post-reionization plasma is much harder to detect. Its intensity is estimated to be no more than $\sim 10^{-5}\,{\rm MJy\,sr^{-1}}$ at 10 GHz and scales with frequency approximately as $\nu^{-0.1}$. It is thus orders of magnitude below the other signals shown in Fig. 2.

Additional contributions to y could in principle occur before recombination. Although the recombination process is very sensitive to the abundance of ionizing photons, comptonization distortions with $y<0.01$ have no detectable effect on Planck maps (Chluba & Sunyaev, 2009).

2.10 Constraints on distortions from the dipole frequency spectrum

The severe challenge to any attempt at improving by large factors the constraints on distortion parameters represented by foreground contamination motivates the search for methods alternative to absolute measurements and less affected by foregrounds, or at least affected by them in a different way. Two techniques have been proposed to this effect. They are based on measurements of the spectral dependence of the dipole anisotropy and of the SZ effect.

The dipole amplitude is directly proportional to the first derivative of the photon occupation number or of the CMB intensity (Danese & de Zotti, 1981). In the case of a black-body spectrum:

$$\begin{aligned} I_P(\nu) &= \frac{2h\nu^3}{c^2}\frac{1}{e^x-1}\simeq 2.6988\times10^{-15}\frac{x^3}{e^x-1}\ {\rm erg\,cm^{-2}\,s^{-1}\,Hz^{-1}\,sr^{-1}} \\ &\simeq 269.88x^3\eta_{\rm P}\ {\rm MJy\,sr^{-1}}. \end{aligned} \quad (43)$$

The observer moving at velocity V with respect to the CMB sees, *in the direction of*

motion, a temperature

$$T = \frac{\left[1-(V/c)^2\right]^{1/2}}{1-V/c} T_{\rm CMB} \simeq \left(1+\frac{V}{c}\right) T_{\rm CMB}. \tag{44}$$

In the case of a black-body spectrum, the amplitude of the dipole anisotropy has the spectrum

$$\frac{\Delta I_P(\nu)}{I_P(\nu)} = \frac{I_P(\nu,T) - I_P(\nu,T_{\rm CMB})}{I_P(\nu)} \simeq \frac{xe^x}{e^x-1}\frac{V}{c}. \tag{45}$$

The fractional deviations from the perfect black-body case of the frequency dependence of the dipole amplitude for y– and μ–type distortions are very small but future experiments with sensitivities orders of magnitude better than COBE/FIRAS (Fixsen et al., 1996), such as PIXIE and COrE+[1] could provide interesting checks or even improve on COBE/FIRAS absolute measurements.

In the presence of CMB spectral distortions, the frequency spectrum of the SZ effect changes as (Wright, 1983)

$$\frac{\partial I}{\partial y} = \frac{\partial^2 I}{\partial^2 \ln \nu} - 3\frac{\partial I}{\partial \ln \nu}. \tag{46}$$

The effect of distortions discussed above on the shape of the SZ effect is hardly detectable. The reason for that is easily understood: the second derivative emphasizes sharp spectral features while the distorted spectra we have considered are relatively smooth. In fact the main application of this method was thought to be a test of the steep excess around the CMB peak reported by Woody et al. (1975).

3 CMB anisotropies

3.1 The dipole

The CMB is remarkably uniform. Apart from the dipole induced by our own motion (Smoot et al., 1977), it took 28 years of efforts to reach the first detection, by the COBE/DMR, of primordial anisotropies (Smoot et al., 1992).

The currently most precise value of the dipole amplitude has been obtained from *Planck* data (Planck Collaboration, 2015c) (stat and sys stand for statistical and systematic errors, respectively):

$$(\Delta T)_{\rm dipole} = 3364.46 \pm 0.006\,({\rm stat}) \pm 0.8\,({\rm sys})\,\mu{\rm K} \tag{47}$$

or

$$\left(\frac{\Delta T}{T}\right)_{\rm dipole} = (1.2347 \pm 0.0029) \times 10^{-3} \tag{48}$$

towards $l = 263^\circ.94 \pm 0^\circ.001\,({\rm stat}) \pm 0^\circ.010\,({\rm sys})$, $b = 48^\circ.213 \pm 0^\circ.001\,({\rm stat}) \pm 0^\circ.002\,({\rm sys})$ (latitude and longitude in Galactic coordinates). This implies a Solar System peculiar velocity of $370.5 \pm 0.5\,{\rm km\,s^{-1}}$ with respect to the CMB rest frame.

[1] `http://www.core-mission.org/documents/CoreProposal_Final.pdf`

An observer moving at velocity $\vec{V}$ with respect to the CMB frame sees, in the direction defined by the unit vector $\vec{e}$, a photon with proper energy $h\nu$ Doppler shifted to the energy

$$h\nu' = h\nu\gamma\left(1 + \frac{\vec{V}}{c}\cdot\vec{e}\right) = h\nu\gamma\left(1 + \beta\cos\theta'\right) \tag{49}$$

where $\beta = V/c$ and θ' is the angle in the *observer*'s frame and γ is the Lorentz factor:

$$\gamma = \frac{1}{\sqrt{1-\beta^2}}. \tag{50}$$

If the *intrinsic* spectrum is a blackbody at $T_{\rm CMB}$, the *observed* photon distribution function is

$$\eta'(\theta) = \frac{1}{\exp\frac{h\nu}{kT_{\rm obs}} - 1} \tag{51}$$

with

$$T_{\rm obs}(\theta) = \frac{T_{\rm CMB}}{\gamma\left(1 + \beta\cos\theta\right)}. \tag{52}$$

Thus the spectrum still looks like a blackbody along any direction but the observed temperature varies with direction. Expanding to second order in β we find

$$T_{\rm obs}(\theta) = T_{\rm CMB}\left(1 + \beta\cos\theta + \frac{1}{2}\beta^2\cos(2\theta)\right) \tag{53}$$

so that the motion also induces a quadrupole anisotropy of order β^2.

3.2 Small-scale anisotropies

The detected small-scale temperature fluctuations, $\Delta T/T$, are at the 10^{-5} level, in stark contrast to the matter in the Universe, organized in very nonlinear structures. The disparity between the smooth photon distribution and the clumpy matter distribution is due to radiation pressure. Matter inhomogeneities grow owing to gravitational instability, but pressure prevents the same process from occurring in the photons.

The growth rate of density perturbations in the linear regime of non-relativistic component is at most as fast as $a = 1/(1+z)$. Recombination took place at $z \simeq 1000$. Thus, with no dark matter, the present-day amplitude of typical fractional overdensities should be ~ 0.01. But galaxies and galaxy clusters have fractional overdensities $\gg 1$. Hence fluctuations that we see in the CMB are not enough to account for the structure we see today unless potential fluctuations at recombination were much larger than CMB temperature fluctuations. Such potential fluctuations are provided by dark matter.

In the currently standard scenario, the dark matter is not coupled to photons and baryons, so its fluctuations can grow independently. When a perturbation enters the horizon, its baryon-photon component stops growing: its starts oscillating in the dark matter potential wells. The amplitude of their (small) fluctuations is what we see to be as $\Delta T/T \sim 10^{-5}$. On the contrary, dark matter overdensities continue to grow so that, at recombination, they are much larger than those of the baryon-photon fluid; but we do not see them directly. At recombination baryons decouple

from photons and fall into the dark matter potential wells, thus suddenly increasing their overdensity, while radiation free-streams to us. Thus, *the amplitude of CMB fluctuations directly imply dark matter* and even though both inhomogeneities in the matter and anisotropies in the CMB apparently originated from the same source, these appear very different today.

Because the photon distribution is very uniform, perturbations are small, and *linear theory applies. This is perhaps the most important fact about CMB anisotropies.* Because they are linear, predictions can be made as precisely as their sources are specified. Sources of the anisotropies are also linear fluctuations, so their relationships to the cosmological model are governed by simple, well understood physics, unlike other cosmological observations that are afflicted by a host of non-linear astrophysical processes.

This allows extremely precise determinations of cosmological parameters. But we will see that other cosmological observations are nevertheless necessary to break degeneracies among parameter values. Although the physics is simple and well understood, calculations at the level of accuracy required by the high quality CMB maps available today is complicated. There are several components in the primordial soup prior to recombination: baryons, photons, electrons, neutrinos and dark matter particles.

Each component obeys its own Boltzmann transport equations that describe how the phase space density of each component changes with time in the presence of interactions with other species. Because of interactions all these equation are coupled; to get the CMB spectrum they have to be evolved together from an early epoch, through recombination. Codes exist to do that, the best known are probably CMBFAST[2] and CAMB[3]. These lectures will avoid these complications and focus on the basic physics.

3.3 Physics of primordial CMB temperature anisotropies: generalities

The current state-of-the-art data-set is the one provided by the *Planck* satellite (Planck Collaboration, 2015a). Various component separation techniques have been applied to *Planck* multi-frequency maps to extract CMB temperature and polarization maps as clean as possible, removing the diffuse emissions of astrophysical origin, referred to as "foregrounds" (Planck Collaboration, 2015b).

Let us now consider the temperature map. It gives us the CMB intensity (or, equivalently, the CMB temperature) as a function of the direction on the sky. It is convenient to expand the temperature fluctuation map in spherical harmonics, $Y_{lm}(\theta, \phi)$, equivalent, on a spherical surface, to the Fourier expansion on the plane:

$$\Delta T(\theta, \phi) = \sum_{1}^{\infty} \sum_{m=-\ell}^{\ell} a_{lm} Y_{lm}(\theta, \phi). \tag{54}$$

Although the sum runs over $\ell \geq 1$, the dipole ($\ell = 1$) is usually subtracted since it is of local origin.

The statistical properties of the fluctuations in a perturbed cosmology should respect the symmetries of the background model. The cosmological principle implies

[2] `http://lambda.gsfc.nasa.gov/toolbox/tb_cmbfast_ov.cfm`
[3] `http://lambda.gsfc.nasa.gov/toolbox/tb_camb_ov.cfm`

that the statistics should be independent of spatial position (homogeneous) and invariant under rotations of the field. Demanding invariance under rotations fixes the second-order statistics to be of the form

$$\langle a^*_{l'm'} a_{lm} \rangle = C_\ell \delta_{\ell\ell'} \delta_{mm'}, \tag{55}$$

where the C_ℓ's are the *power spectrum*:

$$C_\ell = \langle |a_{\ell m}|^2 \rangle = \frac{1}{2\ell+1} \sum_m |a_{\ell m}|^2. \tag{56}$$

Angle brackets denote an average over many realizations and the $*$ denotes the complex conjugate. Equation (55) tells us that the a_{lm}'s are uncorrelated for different values of ℓ and m.

If the fluctuations are also Gaussian, as predicted by the simplest inflationary models, all higher order statistics vanish so that

- the power spectrum provides a complete statistical description of anisotropies,
- the a_{lm}'s, hence the C_ℓ's are independent.

In the real space the temperature fluctuations can be quantified using the correlation function computed averaging the product of temperature fluctuations in all pairs of directions $\overrightarrow{\theta_1}$ and $\overrightarrow{\theta_2}$ separated by the angle θ:

$$C(\theta) = \langle \Delta T(\overrightarrow{\theta_1}) \Delta T(\overrightarrow{\theta_2}) \rangle. \tag{57}$$

The fact that the correlation function depends only on the modulus of the angular separation θ and not on its direction is again a consequence of the rotational invariance. The two descriptions are related by

$$C(\theta) = \frac{1}{4\pi} \sum_\ell (2\ell+1) C_\ell P_\ell(\cos\theta), \tag{58}$$

where the P_ℓ's are the Legendre polynomials. The statistical independence of the C_ℓ's, unlike the $C(\theta)$'s for different values of θ, makes the power spectrum optimally suited for cosmological investigations.

If anisotropies are Gaussian, the estimates of C_ℓ have a χ^2 distribution with $2\ell+1$ degrees of freedom and variance (Knox, 1995)

$$(\Delta C_\ell)^2 = \frac{2}{2\ell+1} C_\ell^2. \tag{59}$$

The factor $2\ell+1$ follows from the fact that this is the number of m-samples of the power in each multipole moment ℓ, and the factor of 2 in the numerator is because the variance of a χ^2-distributed variable is twice the expectation number.

Equation (59) quantifies the fundamental limitation called "cosmic variance", endowed with the nature of the C_ℓ's that are averages over many realizations, but we actually have only one realization of the universe. Thus the precision in the power spectrum determination decreases with ℓ, irrespective of the accuracy of measurements.

Of course, an additional contribution to ΔC_ℓ comes from instrumental and astrophysical sources of noise. If the noise is also Gaussian, one has

$$\frac{\Delta C_\ell}{C_\ell} = \left(\frac{4\pi}{A}\,\frac{2}{2\ell+1}\right)^{1/2}\left(1+\frac{A\sigma^2}{N\,C_\ell\,W_\ell}\right), \tag{60}$$

where A is the usable area of the sky, σ is the rms pixel noise, N is the number of pixels in the map and W_ℓ is the window function.

It is usual to relate the multipole number ℓ to the angular scale θ as $\ell \simeq \pi/\theta$, with θ in rad. This works well at the lowest multipoles because it correctly associates $\ell = 1$ to $\theta = \pi$ and $\ell = 2$ to $\theta = \pi/2$. However, this relation becomes misleading at high ℓ.

For large ℓ's, in correlation function arguments we find $\ell + 1/2 \approx 1/[2\sin(\theta/2)]$. For small θ (i.e. for $\ell \gg 1$) this becomes $\ell \approx 1/\theta$ with θ in radians or $\ell \approx 57.3/\theta$ with θ in degrees (see also White et al., 1994, who give $\ell \approx 60^\circ/\theta$).

As suggested by eqs. (57) and (58), the mean square temperature fluctuation over an instrumental solid angle $\omega = 2\pi\theta^2$ is

$$\langle(\Delta T(\theta))^2\rangle = C(0) = \omega^2 \sum_\ell \frac{2\ell+1}{4\pi} W_\ell C_\ell \simeq \omega^2 \int \frac{\ell^2}{2\pi} C_\ell W_\ell d\ln\ell, \tag{61}$$

where W_ℓ is the window function describing the ℓ-space region observable with the considered instrument. For a Gaussian instrument beam with FWHM $= 2\sqrt{2\,\ln 2}\sigma_b$, $W_\ell = \exp(-\ell^2\sigma_b^2)$. Thus the quantity

$$D_\ell = \frac{\ell(\ell+1)}{2\pi} C_\ell \tag{62}$$

is approximately the power of temperature anisotropies per $\Delta\ln\ell = 1$. D_ℓ is the quantity that is frequently plotted instead of C_ℓ.

3.4 Physics of primordial CMB temperature anisotropies: anisotropy sources

CMB anisotropies arise at recombination and during the subsequent free-streaming of photons and are due to several effects:

- temperature variations present at recombination (higher photon energy density $\Rightarrow$ higher CMB temperature);
- gravitational redshift of photons;
- time-variable gravitational potential;
- Doppler shifts from fluid motion at last scattering;
- gravitational waves (tensor fluctuations).

There are three critical scales, all defined at recombination:

- the sound horizon;
- the width of the last scattering shell;

- the damping scale.

The *comoving* size of the sound horizon at recombination is the distance the sound could travel from $t = 0$ to recombination time $t_{\rm rec}$. Compressional waves propagate as disturbances in pressure and density. Hence the speed of sound is:

$$c_s^2 = \frac{dp}{d\rho}. \tag{63}$$

In the early universe radiation and baryons are coupled together through frequent photon-electron scatterings, combined with coupling between protons and electrons. Dark matter, which is most probably collisionless, i.e. does not interact with anything except through gravity, would not participate in the pressure and density disturbances.

The sound speed in the early Universe depends on baryons and radiation, so

$$c_s^2 = \frac{(dp/dT)_{\rm rad} + (dp/dT)_{\rm baryons}}{(d\rho/dT)_{\rm rad} + (d\rho/dT)_{\rm baryons}}. \tag{64}$$

Non-relativistic matter has (almost) no pressure. To be precise, for baryons,

$$\begin{aligned} w &= p/\rho = \frac{n_e kT_e + n_p kT_p}{n_e m_e c^2 + n_p m_p c^2 + \frac{3}{2} n_e kT_e + \frac{3}{2} n_p kT_p} \\ &\simeq \frac{2kT_e}{m_p c^2} \simeq 5.5 \times 10^{-10} \frac{1+z}{1100} \end{aligned} \tag{65}$$

Hence, $(dp/dT)_{\rm baryons} \simeq 0$. The other terms can be evaluated because we know that $p = w\rho$ (for the radiation $w = 1/3$), $\rho = \rho_0 a^{3(1+w)}$ and $T \propto a^{-1}$, where $a \propto (1+z)^{-1}$ is the scale factor. The result is:

$$c_s^2 = c^2 \frac{(4/3)\rho_r}{4\rho_r + 3\rho_b} = \frac{c^2}{3(1+R)}, \tag{66}$$

where $R = 3\rho_b/4\rho_r$. For pure radiation ($R = 0$) $c_s^2 = c^2/3$. Compared to that, baryons have the effect of lowering the sound speed. At the other extreme, $R \gg 1$, we get

$$c_s^2 = c^2 \frac{4\rho_r}{9\rho_b} \simeq 1.1 \times 10^{-5} \frac{c^2(1+z)}{h^2 \Omega_b}, \tag{67}$$

implying that the sound speed decreases considerably with cosmic time. Since $\rho_b \simeq 4.2 \times 10^{-31}(1+z)^3\,{\rm g\,cm^{-3}}$ and $\rho_r = a_{\rm bb} T_{\rm CMB}^4 \simeq 4.6 \times 10^{-34}(1+z)^4\,{\rm g\,cm^{-3}}$, at $z_{\rm rec} \simeq 1100$ we have $R = 3\rho_b/4\rho_r \simeq 0.6$, so that we are in an intermediate situation.

Note that the canonical equivalence redshift is ***not*** defined by $\rho_b(z) = \rho_r(z)$ but by $\rho_{\rm non\,relativistic}(z_{\rm eq}) = \rho_{\rm relativistic}(z_{\rm eq})$, where $\rho_{\rm non\,relativistic}$ includes the contribution of dark matter and $\rho_{\rm relativistic}$ includes the contribution of neutrinos that, given the tight constraints on their masses, discussed in the following, must be relativistic at $z_{\rm eq}$. In the standard cosmological model $\rho_{\rm relativistic} \simeq 1.68\rho_r$ and $z_{\rm eq} \simeq 3420$.

Hence, the *comoving* size of the sound horizon at recombination is

$$r_s = \int_0^{t_{\rm rec}} (1+z) c_s\, dt = \int_{z_{\rm rec}}^{\infty} c_s\,(1+z) \frac{dt}{dz} dz \tag{68}$$

$$\frac{dt}{dz} = a(t)\frac{a(t)}{\dot{a}(t)} \simeq \frac{4.6\times10^{17}(H_0/68)^{-1}}{(1+z)E(z)}\ \mathrm{s}, \tag{69}$$

$E(z) = \left[\Omega_m(1+z)^3 + \Omega_r(1+z)^4 + \Omega_K(1+z)^2 + \Omega_\Lambda\right]^{1/2}$. Since, with the current values of the cosmological parameters, the universe became matter dominated well before recombination, $dt/dz \propto \Omega_m^{-1/2}(1+z)^{-5/2}$. Under this approximation, $r_s \simeq 100(h^2\Omega_m)^{-1/2} \simeq 270\,\mathrm{Mpc}$.

The wavemode that completes half an oscillation by recombination sets the physical scale of the first peak. The observed angular scale corresponding to this physical size depends on the geometry of the universe (see slides): it is larger for a closed universe and smaller for an open one. The BOOMERANG (de Bernardis et al., 2000), MAXIMA (Hanany et al., 2000) and TOCO (Torbet et al., 1999) experiments have found that the first peak is located at $\ell \simeq 200$ (angular scale of $\simeq 1.8^\circ$) as expected for a spatially flat universe. The global density parameter must then be $\Omega \simeq 1$, implying that the cosmic energy density must be dominated by "dark" components.

On super-horizon scales the temperature in any given direction depends only on gravity, i.e. on the depth of the potential, ϕ, through two effects[4]:

$$\begin{aligned}\frac{\Delta T}{T}(\vec{r}) &= \left(\frac{\Delta T}{T}\right)_{\mathrm{grav\,1}} + \left(\frac{\Delta T}{T}\right)_{\mathrm{grav\,2}} \\ &= \phi(\vec{r}) - \frac{2}{3}\phi(\vec{r}) = \frac{1}{3}\phi(\vec{r}).\end{aligned}$$

The first term arises because the curvature due to the gravitational potential is essentially a perturbation to the scale factor. Hence, a change of curvature generates a temperature perturbation in analogy to the cosmological redshift so that $\Delta\nu/\nu = \Delta T/T = \phi$.

The second term is due to the delay, Δt, of photons climbing out of potential wells, and the opposite effect for photons descending from potential peaks. We have $\phi = \Delta t/t$. The photons we see today come from wells as they were during an earlier cosmic epoch, when the average temperature was higher everywhere. Using $\rho \propto a(t)^{-3}$, $a(t) \propto t^{2/3}$ as appropriate in the matter-dominated epoch, and $T \propto a(t)^{-1}$ we see that $\Delta T/T = (-2/3)\Delta t/t = (-2/3)\phi$.

The first effect would make a gravitational potential well appear as a *cold* spot, compared to average temperature. The second effect would make potential wells appear as *warm* spots. The first effect dominates over the second, and so the overall result is that gravitational potential wells (negative ϕ) look colder than average on these large angular scales. The potential peaks appear as warmer than average spots.

The Newtonian potential of a fluctuation from a homogeneous mass distribution is (Peebles, 1993, p. 501):

$$\phi \sim \frac{G\delta M}{R} = \frac{G}{R}\frac{\delta M}{M}\frac{4}{3}\pi\rho_b R^3 \tag{70}$$

so that the rms fluctuations in the gravitational potential are $\phi \propto \sigma_M M^{2/3}$. For a power-law spectrum of density perturbations, $P(k) \propto k^n$, we have

$$\langle\left(\frac{\delta\rho}{\rho}\right)^2\rangle_\lambda \propto k^{n+3} \tag{71}$$

[4]See `http://homepages.spa.umn.edu/~llrw/a5022/f12/CMBnotes.pdf`

and the fluctuation in the mass enclosed within a volume $\lambda^3 \simeq (2\pi/k)^3$ is

$$\sigma_M \propto \langle \left(\frac{\delta\rho}{\rho}\right)^2 \rangle_\lambda^{1/2} \propto M^{-(n/6+1/2)}. \tag{72}$$

Thus

$$\phi \propto \sigma_M M^{2/3} \propto k^{(n-1)/2}. \tag{73}$$

(For angular scales $\ll 1\,\mathrm{rad}$, $k \simeq \ell/2$). Hence the slope of the power spectrum on super-horizon scales, due to the Sachs-Wolfe effect, is a measure of the slope of the power spectrum of primordial perturbations. For a spectrum close to Harrison-Zeldovich($n = 1$), as expected from primordial inflation, the CMB power spectrum,

$$\langle \Delta T^2 \rangle \propto D_\ell \propto \ell(\ell+1)C_\ell \propto \ell^{(n-1)/2} \tag{74}$$

is approximately scale-independent. This is indeed seen in the observed power spectrum (Sachs-Wolfe plateau, see slides). The plateau however is not perfectly flat, implying n slightly smaller than unity ($n = 0.9667 \pm 0.0040$ Planck Collaboration, 2015d).

So far we have learned that

- the angular scale of the first peak implies that the universe is close to spatially flat;
- the Sachs-Wolfe plateau on large scales implies that the primordial perturbation spectrum is approximately Harrison-Zeldovich.

As we already saw, sub-horizon perturbations oscillate until photons and baryons are tightly coupled (i.e. until recombination occurs). Afterwards photons are free-streaming and carry to us a snapshot of the state of the fluid at recombination.

The ℓ-mode that host the maximum fluid compression at recombination is seen as a network of hot and cold spots spaced by the sound horizon, translating into the first peak in the power spectrum. The mode that has half the size of the sound horizon is caught at its maximum rarefaction phase, giving rise to the second acoustic peak.

Both compression and rarefaction contribute to the temperature power spectrum because the sign of ΔT doesn't matter for ΔT^2. In between modes will be caught at the in-between phases, with not so extreme temperature deviations. It is important to distinguish two categories of fluid behavior:

- compression in potential wells and rarefaction in potential peaks; these give rise to the odd-numbered peaks (1st, 3rd, etc) in the CMB temperature power spectrum,
- rarefaction in potential wells and compression in potential peaks; these give rise to the even-numbered peaks (2nd, 4th, etc.).

(Remember that potential wells and peaks are determined by dark matter that does not take part in oscillations.) There is an important difference between these two. In the presence of baryons rarefactions in potential wells, peaks cannot attain as high an amplitude as compressions because baryons have inertia, and want to stay at the bottoms of potential wells, and away from peaks. So this baryon drag results in the odd peaks having higher amplitude than the even peaks.

There are three contributions to the temperature fluctuations: gravitational frequency shift, temperature change due to the compression or rarefaction of the fluid, and the Doppler term due to the motion of the fluid:

$$\begin{aligned}\frac{\Delta T}{T}(\vec{r}) &= \left(\frac{\Delta T}{T}\right)_{\rm grav} + \left(\frac{\Delta T}{T}\right)_{\rm thermal} + \left(\frac{\Delta T}{T}\right)_{\rm Doppler} \\ &= \phi + \frac{1}{3}\frac{\delta\rho}{\rho} - v_{\parallel}\end{aligned}$$

The first term is the usual gravitational frequency shift. It does not evolve much during the relatively short recombination period, and also because dark matter is not tied to the baryon-photon fluid. The second term comes in because the photons are coupled to the baryons. Thus the densities of the two scale proportionately, $n_\gamma \propto n_b$. For black body radiation the number density of photons, $n_\gamma \propto T^3$, so $\rho_b = n_b m_b \propto T^3$, and differentiating, $\Delta T/T = (1/3)\Delta\rho_b/\rho_b$.

In the Fourier space each k-mode evolves independently, in the linear regime. The equation for the evolution of linear density perturbations is

$$\ddot{\delta_k} + 2(\dot{a}/a)\dot{\delta}_k + (c_s^2 k^2 - 4\pi G\rho)\delta_k = 0. \tag{75}$$

The second term on the left-hand side comes from the Hubble expansion and can be neglected if the fluctuations are much smaller than the horizon (expansion timescale much larger than the fluctuation timescale).

Furthermore, the Poisson equation gives $-4\pi G\rho\delta_k = k^2\phi_k$ so that we have

$$\ddot{\delta_k} + c_s^2 k^2 \delta_k + k^2\phi_k = 0 \tag{76}$$

which is an equation of a driven harmonic oscillator, with a constant driving force provided by the gravitational potential. Its solution is

$$\delta_k = A\cos c_k t + B. \tag{77}$$

(Since $\dot{\delta}_k$ should be zero at early times, we can discard the sine solution.) B can be determined computing $\dot{\delta}_k$ and $\ddot{\delta}_k$ and plugging them into eq. (75) to get: $B = -\phi_k/c_s^2 = -3\phi_k(1+R)$. A can be computed taking into account that

$$\left(\frac{\Delta T}{T}\right)_{k,\rm grav} + \left(\frac{\Delta T}{T}\right)_{k,\rm thermal} = \phi_k + \frac{\delta_k}{3} \tag{78}$$

and that, for $k \to 0$ (large scales), $(\Delta T/T)_k = \phi_k/3$ (Sachs-Wolfe limit).

For $k \to 0$ $\delta_k = A + B$. Combining: $\phi_k/3 = \phi_k + \frac{1}{3}(A+B)$, whence $A = \phi_k(1/c_s^2 - 2) = \phi_k(1+3R)$. Thus

$$\left(\frac{\Delta T}{T}\right)_{k,\rm grav} + \left(\frac{\Delta T}{T}\right)_{k,\rm thermal} = \frac{1+3R}{3}\phi_k\cos(c_s k t) - R\phi_k. \tag{79}$$

Values of $(c_s kt) = \pi$, 3π, 5π, ... ($\cos(c_s kt) = -1$) correspond to the 1st, 3rd, 5th, ... acoustic peaks, while $(c_s kt) = 2\pi$, 4π, 6π, ... correspond to the 2nd, 4th, 6th, ... peaks. The amplitude of odd peaks is thus

$$\left(\frac{\Delta T}{T}\right)_{k,\rm grav} + \left(\frac{\Delta T}{T}\right)_{k,\rm thermal} = \frac{1+3R}{3}\phi_k. \tag{80}$$

The amplitude of even peaks is smaller:

$$\left(\frac{\Delta T}{T}\right)_{k,\mathrm{grav}} + \left(\frac{\Delta T}{T}\right)_{k,\mathrm{thermal}} = \frac{1}{3}\phi_k, \tag{81}$$

Thus the amplitude of odd peaks is enhanced by a factor $(1+6R)$ compared to a no-baryon case and to even peaks. This explains why the amplitude of the second peak is so much smaller than that of the first peak.

On the other hand, the amplification is reduced for higher odd peaks since $R \to 0$ as we go to earlier times, i.e. as the epoch at which oscillations started goes towards radiation dominance. That's why the third peak is also lower than the first peak. Nevertheless, the relative peak heights probe $h^2\Omega_b$ through R. At constant ϕ, the amplitude ratios between neighbouring odd- and even-numbered peaks is $(3+6R)$

Let's now turn to the Doppler term. The velocity of the fluid due to its oscillations can be obtained using continuity equation which relates the rate of change of density to the divergence of the velocity: $d\rho/dt = -\rho\vec{\nabla}\cdot\vec{v}$. The linear perturbation theory gives

$$\dot{\delta} = -\vec{\nabla}\cdot\vec{v} = -\vec{\nabla}\cdot\sum_k \delta_v e^{-i\vec{k}\cdot\vec{r}} = \sum_k -i\vec{k}\cdot\vec{v}_k, \tag{82}$$

in physical coordinates. The two last steps show that if the velocity field can be represented as a Fourier sum over independently evolving k-modes, then taking the spatial gradient is the same as multiplication by $-i\vec{k}$. Because we are dealing with each k-mode separately, the above equation allows us to relate δ_k and $\vec{v}_k$:

$$\dot{\delta}_k = -\vec{\nabla}\cdot\vec{v_k} = -i\vec{k}\cdot\vec{v}_k. \tag{83}$$

The i factor says that these fluctuations are $\pi/2$ out of phase with the density-induced temperature fluctuations.

In turn, $\dot{\delta}_k$ can be obtained differentiating the expression derived above:

$$\delta_k = (1+3R)\phi_k\cos(c_s k t) - 3(1+R)\phi_k. \tag{84}$$

Statistically speaking, all three spatial directions have the same contribution to the velocity dispersion, so the Doppler line-of-sight contribution due to the motion of the fluid is:

$$\left(\frac{\Delta T}{T}\right)_{k,\mathrm{Doppler}} = \frac{|\vec{v}_k|}{\sqrt{3}} = \frac{1+3R}{[3(1+R)]^{1/2}}\phi_k\sin(c_s k t). \tag{85}$$

In the absence of baryons ($R=0$), the gravitational + thermal and the Doppler effect are of equal amplitude and $\pi/2$ out of phase, i.e. go as the cosine and sine of the same angle and so, when added in quadrature we would obtain a flat, scale independent power spectrum. In other words a scale invariant initial temperature spectrum would lead to a scale invariant spatial power spectrum at recombination.

Baryons break that symmetry because they definitely prefer the bottoms of potential wells, and so enhance the amplitude of compressions in the wells, and rarefactions at the potential peaks, over the reverse situations. The maximum amplitude of Doppler peaks is

$$\left(\frac{\Delta T}{T}\right)_{k,\mathrm{Doppler}} = \frac{1+3R}{[3(1+R)]^{1/2}}\phi_k. \tag{86}$$

Baryons also enhance the Doppler term, but not as much as the gravitational potential term.

The Doppler effect also carries an angular dependence that changes its projection on the sky: it vanishes when the observer is looking perpendicular to $\vec{v}\|\vec{k}$ whereas it is in that direction that the acoustic peaks in temperature gain most of their contribution. So in angular space, projection effects distribute the power over a range of multipoles, smoothing the Doppler features.

Thus, the Doppler effect provides spatial fluctuations of comparable strength to the local temperature fluctuations from acoustic oscillations (lower) providing features at the troughs of the latter. However, these are not directly observed. What we see are fluctuations in angular space where projection effects smooth the Doppler features leaving a morphology that reflects the temperature oscillations.

In summary, which information do we obtain from peaks in the CMB power spectrum (see Hu, 2008)?

First peak: curvature and dark energy. The comparison between the predicted acoustic peak scale and its observed angular extent provides a measurement of the angular diameter distance to recombination. The angular diameter distance in turn depends on the spatial curvature and expansion rate of the universe. With the matter and radiation energy densities measured, the remaining contributor to the expansion rate is the dark energy. The other key ingredient is the calibration of the linear scale of the sound horizon at recombination. This depends on baryon-photon momentum density ratio, R, i.e. on Ω_b, and on the expansion rate prior to recombination, determined by the matter/radiation ratio, i.e. by Ω_m. The calibration of these two quantities involves the higher acoustic peaks.

Second Peak: baryons. The baryon-photon ratio controls the even-odd modulation of peak heights through the baryon loading effect. The second peak represents rarefaction of the acoustic wave in a gravitational potential and hence is suppressed in amplitude by the baryon inertia. But also the dark matter density plays a role. To see this, suppose that the universe is radiation-dominated. Then, when a perturbation reached maximum compression, as it expanded out the photons would continue to redshift, hence the gravitational potential would decay away. This would allow the temperature perturbation to be much greater than it would otherwise, and hence would enhance the peaks. In contrast, nonrelativistic matter does not redshift, so the gravitational potential it produces does not redshift away. This would lead to relatively smaller fluctuations and smaller peaks.

Third Peak: Dark Matter. The third peak shows the effects of the matter-radiation ratio on the overall amplitude of the acoustic peaks. The universe only becomes matter dominated in the few e-folds before recombination. Peaks corresponding to wavenumbers that began oscillating earlier carry the effects of the prior epoch of radiation domination, when the decay in the gravitational potential would reduce the baryon loading effect and change the peak height ratios. The observed height of the third peak indicates that cold dark matter exists, dominates the energy density at recombination but is not enough to provide the critical density.

The damping tail. Small scales are affected by a number of effects, all of which smear the fluctuations, thereby reducing the amplitude of the CMB power spectrum at large ℓ. An important parameter is the thickness of the last scattering shell, as discussed in the following. Projection from the 3D distribution to the 2D ℓ-mode description also have a role.

3.4.1 The last scattering shell and the damping scale

The electron scattering optical depth for $z_r > z_{\rm rec} \simeq 1100$ and a fully ionized plasma is

$$\begin{aligned} \tau_{\rm es}(z_r) &= \int_{z_{\rm rec}}^{z_r} n_e\, \sigma_T\, (1+z)^{-1} \frac{c}{H(z)}\, {\rm d}z \\ &\simeq 800 \left[\left(\frac{z_r}{z_{\rm rec}} \right)^{3/2} - 1 \right], \end{aligned} \tag{87}$$

implying a quick damping of any anisotropy. As the recombination proceeds, the optical depth sinks down as (Peacock, 1999)

$$\tau_{\rm es}(z) \simeq 0.37 \left(\frac{z}{1000} \right)^{14.25}. \tag{88}$$

Because $\tau_{\rm es}$ changes rapidly with z, the distribution function for the redshift at which photons were last scattered,

$$e^{-\tau_{\rm es}(z)} \frac{d\tau_{\rm es}}{dz}, \tag{89}$$

is sharply peaked and well represented by a Gaussian with $\langle z \rangle \simeq 1065$ and standard deviation $\sigma_z \simeq 80$, corresponding to a comoving radius

$$\sigma_r \sim 7 (h^2 \Omega)^{-1/2}\, {\rm Mpc}. \tag{90}$$

or to an angular scale of (Peacock, 1999)

$$\theta_r \sim 4 \Omega^{1/2}\, {\rm arcmin}. \tag{91}$$

This is analog to the photosphere of a star: we observe a slice of the temperature field at the radius of last scattering. Features on scales smaller than the thickness of the recombination layer have several of their wavelengths projected onto the sky to get the contribution to a given ℓ mode, and the resulting smearing reduces the amplitude of fluctuations we observe.

As recombination progresses the coupling between photons and baryons gets less tight, so photons tend to diffuse out. The mean free path of photons at recombination is $l_p = \sigma_r$, the width of the last scattering surface. The number of scatterings undergone by photons within one expansion timescale is $n_{\rm sc} \sim r_s / l_p$, where r_s is the horizon size at recombination [eq. (68)].

The total comoving mean-squared distance that a photon will have moved by such a random walk is $l_d \sim n_{\rm sc}^{1/2} l_p = (r_s l_p)^{1/2} \sim 30\,{\rm Mpc}$. Since the angular diameter distance to decoupling is $\sim 14\,{\rm Gpc}$, this corresponds to an angular scale of $\sim 7'$. Photon diffusion damps the amplitude of temperature fluctuations on scales $< l_d$ i.e. beyond the 3rd peak. The damping angular scale is sensitive to Ω_b, that determines l_p, and to Ω_b though r_s and the angular diameter distance. Thus its measurement provides additional important checks on the overall theory.

3.5 Secondary anisotropies

In addition to the primary anisotropies, produced at recombination, there are a number of secondary processes that happen to the photons as they travel from the surface of last scattering to the observer. These include gravitational effects and various scattering effects operating after the onset of re-ionization. Since the effect of gravity on photons is achromatic, the frequency dependence of all gravitational secondary anisotropies follows that of the primary anisotropies.

Gravitational secondary effects include:

- the integrated Sachs-Wolfe effect (ISW);
- the Rees-Sciama and moving halo effects;
- weak gravitational lensing.

Scattering effects include:

- the thermal and kinematic SZ effects;
- the Ostriker-Vishniac effect.

3.5.1 The integrated Sachs-Wolfe effect

The ISW effect is due to the temporal variation of the gravitational potentials along the line of sight. If a potential well were to deepen as a photon crossed it, the photon would receive a net redshift, and there would be a decrement to the CMB temperature along the line of sight. Conversely, a decaying potential well gives a temperature increment.

In the linear regime there are 2 sources of the ISW. Soon after recombination the gravitational potentials of wells and peaks are decaying because photons are free-streaming and thus are removing their contribution to the potential depth (early ISW). The time derivative, $\dot{\phi}_k$, of the potential on a given scale in Fourier space is related to the matter density via the Poisson equation:

$$\phi_k = -\frac{3}{2}\Omega_m \left(\frac{H_0}{k}\right)^2 \frac{\delta}{a(t)}. \tag{92}$$

In a flat, matter dominated universe, density fluctuations grow as $\delta \propto a(t)$ so that $\phi_k = \text{const}$, $\dot{\phi}_k = 0$ and there is no ISW effect. However, since $\Omega_m \simeq 0.3$, the dynamics of the universe at z substantially below unity (for a quantitative estimate of the limiting redshift see below) is no longer controlled by the matter density, as can be seen from consideration of the expansion timescale:

$$\tau_{\rm exp} = \frac{a(t)}{\dot{a}(t)} \simeq \frac{4.6 \times 10^{17} (H_0/68)^{-1}}{\left[\Omega_m(1+z)^3 + \Omega_r(1+z)^4 + \Omega_k(1+z)^2 + \Omega_\Lambda\right]^{1/2}} \text{ s}. \tag{93}$$

At the onset of dark energy (or spatial curvature, in a low density universe) dominance the expansion rate of the universe increases, hence $\delta/a(t)$ decreases, reducing the amplitude of gravitational potential. The differential redshift of the photons climbing in and out of the potential gives rise to a net temperature anisotropy.

There is one qualitative difference between the early ISW and the late ISW effects. For the late ISW effect, the potential decays over a much longer time (of the order of the present day Hubble time). Thus the photons associated to perturbations much smaller than the horizon size have to travel through multiple peaks and troughs of the perturbations and the chances of cancellation of the coherence in gravitational redshifts becomes greater leaving little net perturbation to the photon temperature (Tuluie et al., 1996).

Thus the late ISW effect is seen mainly in the lowest ℓ-values (largest scales) in the power spectrum. The relevant scale is the curvature scale freeze-out in concordance cosmology: the horizon at $z \sim (\Omega_\Lambda/\Omega_m)^{1/3} - 1 \simeq 0.3$. This corresponds to an angular scale of about 10°. Its importance comes from the fact that it is sensitive to the amount, equation of state and clustering properties of the dark energy.

Detection of such a signal is, however, limited by cosmic variance. The time evolution of the potential that gives rise to the ISW effect may also be probed by observations of large-scale structure. One can thus expect the ISW to be correlated with tracers of large-scale structure. This idea was first proposed by Crittenden & Turok (1996) and has been widely discussed in the literature. The *Planck* data have been recently used in combination with many large scale-structure tracers to detect the ISW signal (Planck Collaboration, 2015f). A $4\,\sigma$ detection was achieved. Conditional probability distributions on Ω_Λ and on the parameter w characterizing the equation of state of the dark energy were derived from the ISW likelihood, based on the CMB–large scale structure cross-correlations. The results are consistent with those derived, with much smaller errors, from the analsis of the CMB power spectrum.

3.5.2 The Rees-Sciama effect

Cancellations of the ISW on small spatial scales or in a flat matter-dominated universe leave second-order and non-linear effects. In hierarchical structure formation, the non-linear collapse of a structure can present a changing gravitational potential to passing photons. If the photon crossing time is a non-negligible fraction of the evolution time-scale, the net effect of the blue and redshift is different from zero and the path through the structures leaves a signature on the CMB. This was first pointed out by Rees & Sciama (1968) for evolving density profiles of any individual large-scale structure (see Aghanim et al., 2008, for a review).

3.5.3 The moving halo effect

For an isolated collapsed structure, there can be a change in the gravitational potential along the line of sight due to its bulk motion across the line of sight. The CMB photons entering ahead of a moving structure (galaxy cluster or super-cluster) traversing the line of sight will be red-shifted, while those entering the structure wake are blue-shifted. The transverse motion induces a bipolar imprint in CMB whose amplitude is proportional to the velocity and to the depth of the potential well and aligned with the direction of motion.

The bulk motion of dark matter halos of all masses would contribute to this effect but is found to be negligible for all angular scales (Aghanim et al., 1998; Molnar & Birkinshaw, 2000).

3.5.4 Lensing by large scale structure

As CMB photons propagate from the last scattering surface, the intervening large-scale structure can not only generate new secondary anisotropies (Lewis & Challinor, 2006) but can also gravitationally lens the primary anisotropies, magnifying certain patches in the sky and demagnifying others. The deflection arises from the cumulative effect of large-scale structure along the line of sight. The total deflections have an r.m.s. of $\sim 3'$ and is coherent over scales $\sim 1°$, the angle subtended by the typical coherence size of the gravitational potential, $\sim 100\,\mathrm{Mpc}$, at a comoving radial distance half-way to recombination, where lensing is most efficient.

Lensing conserves brightness, simply re-mapping points according to the deflection field. For the temperature anisotropies, this re-mapping leads to a smoothing of the acoustic peaks resulting in fractional changes in the CMB temperature C_ℓ's of around 10% at the troughs by $\ell \sim 2000$. Moreover, it transfers large-scale power to small scales so that it dominates the primary anisotropies for $\ell > 4000$.

CMB lensing has the potential to provide constraints on dark energy, modifications of gravity, and massive neutrinos that are inaccessible with the primary CMB anisotropies alone.

3.5.5 The Sunyaev-Zeldovich (SZ) effects

The SZ effects are caused by the inverse Compton interaction between the CMB photons and the free electrons of a hot ionized gas along the line of sight, primarily in galaxy clusters. The scattering of photons by the random motion of the thermal electrons produces the thermal SZ (tSZ) effect (see Sect. 2.4), which yields the most important contribution to secondary anisotropies, and the kinetic SZ (KSZ) effect which is due to the bulk motion of the electrons. The tSZ has a unique spectral dependence, described by eq. (30).

If the scattering plasma has a bulk motion relative to the CMB a kinetic SZ (kSZ) effect occurs, along with the tSZ effect. In this case the final spectrum remains Planckian since the scattering only Doppler shifts the incident spectrum. In the limit of non-relativistic plasma moving with radial velocity v_r the change in CMB temperature is given by

$$\left|\frac{\Delta T}{T}\right|_K = \frac{v_r}{c}\tau_{\rm clus}, \tag{94}$$

where $\tau_{\rm clus}$ is the scattering optical depth of the plasma cloud (e.g., a galaxy cluster). The ratio of the change in brightness temperatures caused by the kSZ effect and by the tSZ is, in the Rayleigh-Jeans region (remember that the tSZ effect vanishes at 217 GHz), for a large galaxy cluster,

$$\frac{(\Delta T)_K}{(\Delta T)_T} = \frac{1}{2}\,\frac{v_r}{c}\,\left(\frac{kT_e}{m_e c^2}\right)^{-1} \simeq 0.09\frac{v_r}{1000\,\mathrm{km\,s^{-1}}}\left(\frac{kT_e}{10\,\mathrm{keV}}\right)^{-1}. \tag{95}$$

Since typical peculiar velocities are around a few hundred km/s and typical temperatures a few keV, the kinetic effect comes out to be at least an order of magnitude less than the thermal effect. A tentative (1.8–2.5 σ) detection of the kSZ was reported by Planck Collaboration (2015i).

3.6 Effects of re-ionization

The re-coupling of CMB photons to the baryons, via electrons, due to re-ionization causes a fraction of them to be re-scattered. Linearly, re-scattering induces three changes to the photon distribution: suppression of primordial anisotropy, generation of large angle polarization, and a large angle Doppler effect. The latter two suffer cancellation because photons travel through many peaks and troughts (and associated velocity reversal). Nonlinear effects can counter this suppression.

The fraction of re-scattered photons, is $\simeq \tau_{\rm es}$ ($\tau_{\rm es} \simeq 0.066$ according to Planck results; see Sect. 2.9). Then the amplitude of the acoustic peaks is suppressed by a factor $\exp(-\tau_{\rm es}) \simeq 0.94$. Unlike the plasma before recombination, the medium is optically thin, so the mean free path and diffusion length of the photons is of order the horizon itself. New acoustic oscillations cannot form.

3.6.1 Doppler effect

As discussed by Hu & Dodelson (2002), one might naively expect that velocity fields of order $v/c \sim 10^{-3}$ and optical depths of several percent imply a Doppler effect that rivals the acoustic peaks themselves. That this is not the case is the joint consequence of the cancellation analogous to that noted in connection with the late ISW effect and of the fact that, because the Doppler effect comes from the peculiar velocity along the line of sight, it retains no contributions from linear modes with wave-vectors perpendicular to the line of sight. But, as we have seen, these are the only modes that survive cancellation. Consequently, the Doppler effect from re-ionization is strongly suppressed and is entirely negligible for $\ell > 100$.

The Doppler effect can survive cancellation if the optical depth has modulations in a direction orthogonal to the bulk velocity. This modulation can be the result of either density or ionization fluctuations in the gas. Examples of the former include the effect in clusters (tSZ effect) and linear as well as nonlinear large-scale structures.

Optical depth modulation can also come from variations in the ionization fraction. Predictions for this effect are the most uncertain, as it involves both the formation of the first ionizing objects and the subsequent radiative transfer of the ionizing radiation. It is, however, unlikely to dominate the density-modulated effect except perhaps at very high multipoles ($\ell > 10^4$; Hu & Dodelson, 2002).

3.6.2 The Ostriker–Vishniac effect

Ostriker & Vishniac (1986) and Vishniac (1987) pointed out that when the ionization fraction is homogeneous, i.e. reionization is completed, a modulation of the Doppler effect by spatial variations of the density field generates CMB fluctuations. The calculations (see Aghanim et al., 2008, for a review) show that the re-ionization-induced anisotropies are dominated by the Ostriker-Vishniac effect at large angular scales. The contribution from non-linear density perturbations only intervenes at smaller scales with amplitudes of a few μK at $\ell > 1000$.

3.7 Impact of neutrinos on the CMB power spectrum

Both the number of neutrino species and their total mass affect the CMB power spectrum[5].

The effective number of neutrino species, $N_{\rm eff}$, has impact on

- the equivalence redshift, $z_{\rm eq}$ (see Sect. 3.4) since $\rho_{\rm relativistic} \simeq (1 + 0.227 N_{\rm eff})\rho_r$, ρ_r being the equivalent density of CMB photons (remember that $z_{\rm eq}$ is defined by $\rho_{\rm non\,relativistic}(z_{\rm eq}) = \rho_{\rm relativistic}(z_{\rm eq})$);
- the peak amplitude, reduced due to the gravitational coupling with extra free-streaming species; Hu & Sugiyama (1996) estimated $\Delta C_\ell / C_\ell \simeq -0.072 \Delta N_{\rm eff}$;
- the peak location: since neutrinos propagate at c, i.e. faster than c_s, the "effective sound velocity" is enhanced (neutrino drag effect; Bashinsky & Seljak, 2004) so that the peak multipole shifts by $\Delta\ell \simeq -3\Delta N_{\rm eff}$.

As for masses, if the sum over all species, $M_\nu = \sum_i m_{\nu,i}$, is larger than 1.8 eV, neutrinos become non-relativistic before decoupling. They add to the density of non relativistic matter but do not affect the sound speed.

If neutrinos become non-relativistic after decoupling they produce an additional contribution to the early ISW on scale $20 < \ell < 200$ due to variations of the potential when they become non relativistic. The effect has amplitude

$$\frac{\Delta C_\ell}{C_\ell} \simeq \frac{m_\nu}{10\,{\rm eV}} \tag{96}$$

There is also a small effects at $\ell > 200$ due to the fact that neutrinos are not fully relativistic prior to recombination and the late ISW is slightly reduced with increasing M_ν.

4 CMB polarization

In the presence of quadrupole anisotropy, Thomson scattering polarizes the CMB (see Hu & White, 1997). The CMB is only a few percent polarized, so this signal is intrinsically fainter than the temperature anisotropies.

The temperature and polarization pattern of CMB anisotropies form a 2×2 tensor which can be decomposed into a scalar field, usually referred to as the E-mode of polarization, and a pseudo-scalar field, usually referred to as the B-mode of polarization. The E and B mode definitions are chosen by analogy to electric and magnetic fields since B modes have curl and E modes are curl-free.

The E-mode signal is dominated by contributions from the density perturbations in the primordial plasma that are in turn the dominant source of the temperature anisotropy signal. The much weaker B-mode signal has two sources: (i) relic gravitational wave radiation generated in the early universe by inflation and (ii) gravitation lensing of E-mode polarization by intervening structure in the Universe.

Gravitational waves are described by tensor modes, that represent the transverse trace-free perturbations to the spatial metric. The primordial B-mode is the current

[5] See `http://benasque.org/2012cosmology/talks_contr/172_Julien_12.08.16_Benasque.pdf`

holy grail for cosmology since the ratio of the amplitude of the tensor power spectrum relative to the curvature spectrum, which defines the tensor-to-scalar ratio, r, is a measure of the energy scale of inflation, denoted by $V^{1/4}$. We have (e. g. Baumann et al., 2009):

$$V^{1/4} = 1.06 \times 10^{16}\,\mathrm{GeV}\left(\frac{r}{0.01}\right)^{1/4} \tag{97}$$

To date, high-energy physicists only have indirect clues about physics at this scale and they point to energy scales beyond the reach of earth-bound particle accelerators. Thus, if a primordial tensor mode were to be detected, we would be presented with a unique opportunity to use the universe as a high-energy physics laboratory.

The anisotropy power spectra due to tensor perturbations fall sharply on scales that are sub-Hubble at recombination ($\ell > 60$) since the amplitude of gravitational waves decays away as $1/a(t)$ inside the Hubble radius. This limits the power of temperature anisotropies to constrain gravitational waves since the sampling variance of the dominant scalar perturbations is large at low ℓ. Fortunately, CMB polarization provides an alternative route to detecting the effect of gravitational waves on the CMB which is not limited by cosmic variance. Thus polarization provides the only viable route in the near-future for detecting the background of gravitational waves predicted from inflation and therefore to learn on the potential driving the inflation.

The lensing B-mode signal is useful in its own right as a probe of structure in the early Universe. It must also be thoroughly measured and understood if it is to be removed from the inflationary B-mode signal.

Acknowledgements. GDZ wishes to very warmly thank the organizers of the Kielce Cosmology School "Introduction to Cosmology" for inviting him to give these lectures and particularly Piotr Flin, Agnieszka Pollo and their collaborators for their extraordinary hospitality. Work supported in part by ASI/INAF agreement n. 2014-024-R.0.

References

Afshordi, N., *Cyclotron Emission and Thermalization of the CMB Spectrum*, *ArXiv Astrophysics e-prints* (2002), `astro-ph/0202082`

Aghanim, N., Majumdar, S., Silk, J., *Secondary anisotropies of the CMB*, *Reports on Progress in Physics* **71**, 6, 066902 (2008), `0711.0518`

Aghanim, N., Prunet, S., Forni, O., Bouchet, F. R., *Moving gravitational lenses: imprints on the cosmic microwave background*, A&A **334**, 409 (1998)

Aversa, R., et al., *Black Hole and Galaxy Coevolution from Continuity Equation and Abundance Matching*, *ArXiv e-prints* (2015), `1507.07318`

Bashinsky, S., Seljak, U., *Signatures of relativistic neutrinos in CMB anisotropy and matter clustering*, Phys. Rev. D **69**, 8, 083002 (2004), `astro-ph/0310198`

Baumann, D., et al., *Probing Inflation with CMB Polarization*, in S. Dodelson, D. Baumann, A. Cooray, J. Dunkley, A. Fraisse, M. G. Jackson, A. Kogut, L. Krauss, M. Zaldarriaga, K. Smith (eds.) American Institute of Physics Conference Series, *American Institute of Physics Conference Series*, volume 1141, 10–120 (2009), `0811.3919`

Brusa, M., et al., *X-shooter reveals powerful outflows in $z \sim 1.5$ X-ray selected obscured quasi-stellar objects*, MNRAS **446**, 2394 (2015), `1409.1615`

Burigana, C., *Distortions of the CMB Spectrum by Continuous Heating*, in G. L. Chincarini, A. Iovino, T. Maccacaro, D. Maccagni (eds.) Observational Cosmology, *Astronomical Society of the Pacific Conference Series*, volume 51, 554 (1993)

Cen, R., Ostriker, J. P., *Where Are the Baryons? II. Feedback Effects*, ApJ **650**, 560 (2006), astro-ph/0601008

Chluba, J., *Science with CMB spectral distortions*, *ArXiv e-prints* (2014), 1405.6938

Chluba, J., Paoletti, D., Finelli, F., Rubiño-Martín, J. A., *Effect of primordial magnetic fields on the ionization history*, MNRAS **451**, 2244 (2015a), 1503.04827

Chluba, J., Sunyaev, R. A., *Pre-recombinational energy release and narrow features in the CMB spectrum*, A&A **501**, 29 (2009), 0803.3584

Chluba, J., Sunyaev, R. A., *The evolution of CMB spectral distortions in the early Universe*, MNRAS **419**, 1294 (2012), 1109.6552

Chluba, J., et al., *Spectral distortions from the dissipation of tensor perturbations*, MNRAS **446**, 2871 (2015b), 1407.3653

Crittenden, R. G., Turok, N., *Looking for a Cosmological Constant with the Rees-Sciama Effect*, *Physical Review Letters* **76**, 575 (1996), astro-ph/9510072

Danese, L., de Zotti, G., *The relic radiation spectrum and the thermal history of the Universe*, *Nuovo Cimento Rivista Serie* **7**, 277 (1977)

Danese, L., de Zotti, G., *A statistical analysis of the data on the microwave background radiation spectrum*, A&A **68**, 157 (1978)

Danese, L., de Zotti, G., *Dipole anisotropy and distortions of the spectrum of the cosmic microwave background*, A&A **94**, L33 (1981)

de Bernardis, P., et al., *A flat Universe from high-resolution maps of the cosmic microwave background radiation*, Nature **404**, 955 (2000), astro-ph/0004404

de Zotti, G., Massardi, M., Negrello, M., Wall, J., *Radio and millimeter continuum surveys and their astrophysical implications*, A&A Rev. **18**, 1 (2010), 0908.1896

Delabrouille, J., et al., *The pre-launch Planck Sky Model: a model of sky emission at submillimetre to centimetre wavelengths*, A&A **553**, A96 (2013), 1207.3675

Dicke, R. H., Peebles, P. J. E., Roll, P. G., Wilkinson, D. T., *Cosmic Black-Body Radiation.*, ApJ **142**, 414 (1965)

Dole, H., et al., *The cosmic infrared background resolved by Spitzer. Contributions of mid-infrared galaxies to the far-infrared background*, A&A **451**, 417 (2006), astro-ph/0603208

Draine, B. T., Physics of the Interstellar and Intergalactic Medium (2011)

Fabian, A. C., *Observational Evidence of Active Galactic Nuclei Feedback*, ARA&A **50**, 455 (2012), 1204.4114

Field, G. B., Perrenod, S. C., *Constraints on a dense hot intergalactic medium*, ApJ **215**, 717 (1977)

Fixsen, D. J., et al., *The Cosmic Microwave Background Spectrum from the Full COBE FIRAS Data Set*, ApJ **473**, 576 (1996), astro-ph/9605054

Fixsen, D. J., et al., *The Spectrum of the Extragalactic Far-Infrared Background from the COBE FIRAS Observations*, ApJ **508**, 123 (1998), astro-ph/9803021

Fixsen, D. J., et al., *ARCADE 2 Measurement of the Absolute Sky Brightness at 3-90 GHz*, ApJ **734**, 5 (2011)

Genzel, R., et al., *Evidence for Wide-spread Active Galactic Nucleus-driven Outflows in the Most Massive z ~ 1-2 Star-forming Galaxies*, ApJ **796**, 7 (2014), 1406.0183

Gervasi, M., et al., *TRIS. II. Search for CMB Spectral Distortions at 0.60, 0.82, and 2.5 GHz*, ApJ **688**, 24 (2008), 0807.4750

Hanany, S., et al., *MAXIMA-1: A Measurement of the Cosmic Microwave Background Anisotropy on Angular Scales of* $10'$-5°, ApJ **545**, L5 (2000), astro-ph/0005123

Harrison, C. M., et al., *Energetic galaxy-wide outflows in high-redshift ultraluminous infrared galaxies hosting AGN activity*, MNRAS **426**, 1073 (2012), 1205.1801

Hu, W., *Lecture Notes on CMB Theory: From Nucleosynthesis to Recombination*, *ArXiv e-prints* (2008), 0802.3688

Hu, W., Dodelson, S., *Cosmic Microwave Background Anisotropies*, ARA&A **40**, 171 (2002), astro-ph/0110414

Hu, W., Sugiyama, N., *Small-Scale Cosmological Perturbations: an Analytic Approach*, ApJ **471**, 542 (1996), astro-ph/9510117

Hu, W., White, M., *A CMB polarization primer*, New A **2**, 323 (1997), astro-ph/9706147

Illarionov, A. F., Sunyaev, R. A., *Comptonization, characteristic radiation spectra, and thermal balance of low-density plasma*, Soviet Ast. **18**, 413 (1975a)

Illarionov, A. F., Sunyaev, R. A., *Comptonization, the background-radiation spectrum, and the thermal history of the universe*, Soviet Ast. **18**, 691 (1975b)

Khatri, R., Sunyaev, R. A., *Creation of the CMB spectrum: precise analytic solutions for the blackbody photosphere*, J. Cosmology Astropart. Phys. **6**, 038 (2012), 1203.2601

Khatri, R., Sunyaev, R. A., Chluba, J., *Does Bose-Einstein condensation of CMB photons cancel μ distortions created by dissipation of sound waves in the early Universe?*, A&A **540**, A124 (2012a), 1110.0475

Khatri, R., Sunyaev, R. A., Chluba, J., *Mixing of blackbodies: entropy production and dissipation of sound waves in the early Universe*, A&A **543**, A136 (2012b), 1205.2871

Knox, L., *Determination of inflationary observables by cosmic microwave background anisotropy experiments*, Phys. Rev. D **52**, 4307 (1995), astro-ph/9504054

Kogut, A., et al., *The Primordial Inflation Explorer (PIXIE)*, in Society of Photo-Optical Instrumentation Engineers (SPIE) Conference Series, *Society of Photo-Optical Instrumentation Engineers (SPIE) Conference Series*, volume 9143, 1 (2014)

Kompaneets, A. S., *The establishment of thermal equilibrium between quanta and electrons*, *Soviet Physics JETP* **4**, 730 (1957)

Kuhlen, M., Faucher-Giguère, C.-A., *Concordance models of reionization: implications for faint galaxies and escape fraction evolution*, MNRAS **423**, 862 (2012), 1201.0757

Lapi, A., Cavaliere, A., Menci, N., *Intracluster and Intragroup Entropy from Quasar Activity*, ApJ **619**, 60 (2005), astro-ph/0410028

Lapi, A., et al., *Quasar Luminosity Functions from Joint Evolution of Black Holes and Host Galaxies*, ApJ **650**, 42 (2006), astro-ph/0603819

Lewis, A., Challinor, A., *Weak gravitational lensing of the CMB*, Phys. Rep. **429**, 1 (2006), astro-ph/0601594

Mather, J. C., et al., *A preliminary measurement of the cosmic microwave background spectrum by the Cosmic Background Explorer (COBE) satellite*, ApJ **354**, L37 (1990)

Matsumoto, T., et al., *The submillimeter spectrum of the cosmic background radiation*, ApJ **329**, 567 (1988)

Molnar, S. M., Birkinshaw, M., *Contributions to the Power Spectrum of Cosmic Microwave Background from Fluctuations Caused by Clusters of Galaxies*, ApJ **537**, 542 (2000), astro-ph/0002271

Moss, A., Scott, D., *Gravity Heats the Universe*, *International Journal of Modern Physics D* **18**, 2201 (2009), 0903.5330

Nath, B. B., Silk, J., *Heating of the intergalactic medium as a result of structure formation*, MNRAS **327**, L5 (2001), astro-ph/0107394

Ostriker, J. P., Vishniac, E. T., *Generation of microwave background fluctuations from non-linear perturbations at the ERA of galaxy formation*, ApJ **306**, L51 (1986)

Peacock, J. A., Cosmological Physics (1999)

Peebles, P. J. E., Principles of Physical Cosmology (1993)

Penzias, A. A., Wilson, R. W., *A Measurement of Excess Antenna Temperature at 4080 Mc/s.*, ApJ **142**, 419 (1965)

Peterson, J. B., Richards, P. L., Timusk, T., *Spectrum of the cosmic background radiation at millimeter wavelengths*, *Physical Review Letters* **55**, 332 (1985)

Peyraud, J., *Théorie cinétique des plasmas, interaction matière-rayonnement. I. Action d'un rayonnement donné sur la fonction de distribution électronique par l'intermédiaire des chocs Compton.*, *Journal de Physique* **29**, 88 (1968)

Planck Collaboration, *Planck 2013 results. XI. All-sky model of thermal dust emission*, A&A **571**, A11 (2014a), 1312.1300

Planck Collaboration, *Planck 2013 results. XII. Diffuse component separation*, A&A **571**, A12 (2014b), 1303.5072

Planck Collaboration, *Planck 2015 results. I. Overview of products and scientific results*, *ArXiv e-prints* (2015a), 1502.01582

Planck Collaboration, *Planck 2015 results. IX. Diffuse component separation: CMB maps*, *ArXiv e-prints* (2015b), 1502.05956

Planck Collaboration, *Planck 2015 results. VIII. High Frequency Instrument data processing: Calibration and maps*, *ArXiv e-prints* (2015c), 1502.01587

Planck Collaboration, *Planck 2015 results. XIII. Cosmological parameters*, *ArXiv e-prints* (2015d), 1502.01589

Planck Collaboration, *Planck 2015 results. XIX. Constraints on primordial magnetic fields*, *ArXiv e-prints* (2015e), 1502.01594

Planck Collaboration, *Planck 2015 results. XXI. The integrated Sachs-Wolfe effect*, *ArXiv e-prints* (2015f), 1502.01595

Planck Collaboration, *Planck 2015 results. XXV. Diffuse low-frequency Galactic foregrounds*, *ArXiv e-prints* (2015g), 1506.06660

Planck Collaboration, *Planck intermediate results. XXII. Frequency dependence of thermal emission from Galactic dust in intensity and polarization*, A&A **576**, A107 (2015h), 1405.0874

Planck Collaboration, *Planck intermediate results. XXXVII. Evidence of unbound gas from the kinetic Sunyaev-Zeldovich effect*, *ArXiv e-prints* (2015i), 1504.03339

Rees, M. J., Sciama, D. W., *Large-scale Density Inhomogeneities in the Universe*, Nature **217**, 511 (1968)

Ruan, J. J., McQuinn, M., Anderson, S. F., *Detection of Quasar Feedback from the Thermal Sunyaev–Zeldovich Effect in Planck*, ApJ **802**, 135 (2015), 1502.01723

Rybicki, G. B., Lightman, A. P., Radiative processes in astrophysics (1979)

Seiffert, M., et al., *Interpretation of the ARCADE 2 Absolute Sky Brightness Measurement*, ApJ **734**, 6 (2011)

Shankar, F., Weinberg, D. H., Miralda-Escudé, J., *Self-Consistent Models of the AGN and Black Hole Populations: Duty Cycles, Accretion Rates, and the Mean Radiative Efficiency*, ApJ **690**, 20 (2009), 0710.4488

Silk, J., Mamon, G. A., *The current status of galaxy formation*, *Research in Astronomy and Astrophysics* **12**, 917 (2012), 1207.3080

Smoot, G., et al., *An analysis of recent measurements of the temperature of the cosmic microwave background radiation*, ApJ **331**, 653 (1988)

Smoot, G. F., Gorenstein, M. V., Muller, R. A., *Detection of anisotropy in the cosmic blackbody radiation*, *Physical Review Letters* **39**, 898 (1977)

Smoot, G. F., et al., *Structure in the COBE differential microwave radiometer first-year maps*, ApJ **396**, L1 (1992)

Spitzer, L., Physics of Fully Ionized Gases (1962)

Sunyaev, R. A., *The Necessity of a Neutral Hydrogen Period in the Evolution of the Universe*, *Soviet Physics Doklady* **13**, 183 (1968)

Sunyaev, R. A., *The thermal history of the universe and the spectrum of relic radiation*, in M. S. Longair (ed.) Confrontation of Cosmological Theories with Observational Data, *IAU Symposium*, volume 63, 167–173 (1974)

Sunyaev, R. A., Khatri, R., *Unavoidable CMB Spectral Features and Blackbody Photosphere of Our Universe*, *International Journal of Modern Physics D* **22**, 1330014 (2013), 1302.6553

Sunyaev, R. A., Zeldovich, I. B., *Microwave background radiation as a probe of the contemporary structure and history of the universe*, ARA&A **18**, 537 (1980)

Sunyaev, R. A., Zeldovich, Y. B., *The interaction of matter and radiation in the hot model of the Universe, II*, Ap&SS **7**, 20 (1970)

Sutherland, R. S., Dopita, M. A., *Cooling functions for low-density astrophysical plasmas*, ApJS **88**, 253 (1993)

Torbet, E., et al., *A Measurement of the Angular Power Spectrum of the Microwave Background Made from the High Chilean Andes*, ApJ **521**, L79 (1999), astro-ph/9905100

Tornatore, L., Borgani, S., Viel, M., Springel, V., *The impact of feedback on the low-redshift intergalactic medium*, MNRAS **402**, 1911 (2010), 0911.0699

Tortia, E., *Cyclotron Radiation from a Hot Plasma*, *Physics of Fluids* **4**, 1572 (1961)

Tuluie, R., Laguna, P., Anninos, P., *Cosmic Microwave Background Anisotropies from the Rees-Sciama Effect in $\Omega_0 \leq 1$ Universes*, ApJ **463**, 15 (1996), astro-ph/9510019

Van Waerbeke, L., Hinshaw, G., Murray, N., *Detection of warm and diffuse baryons in large scale structure from the cross correlation of gravitational lensing and the thermal Sunyaev-Zeldovich effect*, Phys. Rev. D **89**, 2, 023508 (2014), 1310.5721

Vernstrom, T., Norris, R. P., Scott, D., Wall, J. V., *The deep diffuse extragalactic radio sky at 1.75 GHz*, MNRAS **447**, 2243 (2015), 1408.4160

Vishniac, E. T., *Reionization and small-scale fluctuations in the microwave background*, ApJ **322**, 597 (1987)

Wall, J. V., Chu, T. Y., Yen, J. L., *Measurements of absolute sky brightness temperatures at 320 and 707 MHz.*, *Australian Journal of Physics* **23**, 45 (1970)

White, M., Scott, D., Silk, J., *Anisotropies in the Cosmic Microwave Background*, ARA&A **32**, 319 (1994)

Woody, D. P., Mather, J. C., Nishioka, N. S., Richards, P. L., *Measurement of the spectrum of the submillimeter cosmic background*, *Physical Review Letters* **34**, 1036 (1975)

Wright, E. L., *Was the Big Bang hot?*, in G. O. Abell, G. Chincarini (eds.) Early Evolution of the Universe and its Present Structure, *IAU Symposium*, volume 104, 113–116 (1983)

Zel'dovich, Y. B., Illarionov, A. F., Syunyaev, R. A., *The Effect of Energy Release on the Emission Spectrum in a Hot Universe*, *Soviet Journal of Experimental and Theoretical Physics* **35**, 643 (1972)

Zel'dovich, Y. B., Levich, E. V., *Stationary state of electrons in a non-equilibrium radiation field.*, *Soviet Journal of Experimental and Theoretical Physics Letters* **11**, 35 (1970)

Zeldovich, Y. B., Sunyaev, R. A., *The Interaction of Matter and Radiation in a Hot-Model Universe*, Ap&SS **4**, 301 (1969)

Zizzo, A., Burigana, C., *On the effect of cyclotron emission on the spectral distortions of the cosmic microwave background*, New A **11**, 1 (2005), `astro-ph/0505259`

Zubovas, K., King, A., *Clearing Out a Galaxy*, ApJ **745**, L34 (2012), `1201.0866`